Table 4 Univariate analysis of risk factors for skin change development

Risk factors	Skin changes ($n=20$)	No skin changes ($n=51$)	*P*-value
Total means sacrum temperature (°C), mean ± SD	38·6 ± 0·7	38·4 ± 0·8	0·331
Total means sacrum moisture (au), mean ± SD	45·8 ± 19·8	49·3 ± 17·3	0·464
Total means umbilicus temperature (°C), mean ± SD	37·6 ± 0·9	37·7 ± 0·9	0·570
Total means umbilicus moisture (au), mean ± SD	38·8 ± 18·6	44·9 ± 17·4	0·197
Total difference skin temperature (°C), mean ± SD*	0·9 ± 0·6	0·6 ± 0·8	0·071
Total difference sacrum moisture (au), mean ± SD**	6·9 ± 18·1	4·3 ± 19·0	0·615
Total maximum interface pressure (mmHg), mean ± SD	42·5 ± 21·6†	29·8 ± 11·2‡	0·077
Total mean room temperature (°C), mean ± SD	29·5 ± 1·5	29·8 ± 1·5	0·451
Total mean room moisture (%), mean ± SD	68·4 ± 7·9	66·4 ± 5·7	0·255
Total mean body temperature (°C), mean ± SD	37·0 ± 0·5	36·9 ± 0·7	0·537
Total mean pulse, mean ± SD	82·6 ± 9·9	78·9 ± 16·5	0·357
Total mean systolic blood pressure (mmHg), mean ± SD	131·5 ± 34·1	135·2 ± 28·9	0·652
Total mean diastolic blood pressure (mmHg), mean ± SD	85·6 ± 21·0	85·1 ± 18·9	0·927
Total mean respiratory rate, mean ± SD	22·4 ± 4·3	23·3 ± 4·8	0·480

*Total difference temperature = (mean sacrum temperature) – (mean periumbilical temperature).
**Total difference moisture = (mean sacrum moisture) – (mean periumbilical moisture).
†$n=13$.
‡$n=20$.

Table 5 Multivariate analysis of risk factors for skin change development

	β	*P*-value	Exp(B)	95% CI
Type of sheet	−2·194	0·053	0·111	0·012–1·032
Total mean Braden score	−1·057	0·000	0·347	0·206–0·585
Constant	13·620	0·000	8·228	

Corneometer has been known as a gold standard in measuring skin hydration; however, we are unable to demonstrate the role of skin moisture in the development of pressure ulcers and superficial skin changes. This is because the average room temperature was higher as 30°C and the average room humidity was 60%, which lead to high perspiration on sacrum area in both groups. It was reported that highest hydration values reduce the sensitivity of capacitance method (45). However, Bates-Jensen *et al.* (25) and Guihan *et al.* (46) confirmed that increasing subepidermal moisture is an early sign of development of pressure ulcers.

Role of bed sheet

Pressure ulcers and superficial skin changes occurred in 28% of patients ($n=20$). Of these, 85% ($n=17$) used a standard hospital sheet made of 100% cotton, whereas 15% ($n=3$) used a synthetic fibre sheet ($P=0·089$). The synthetic fibre sheet has three layers: the first layer, which has direct contact with the skin, has permeability to absorb and send moisture to the second layer, while the second layer has a diffusion ability to distribute excessive moisture to the third layer, which then retains it.

According to Derler *et al.* (47), a sheet of synthetic fibre can reduce the coefficient of friction three fold compared with a standard hospital sheet. Textiles play at least three roles in maintaining a favourable microclimate between the patient's skin and the support surface: wicking away perspiration, reducing heat insulation and reducing the coefficient of friction (48,49). Thus, textiles have a role in the prevention or formation of pressure ulcers and other superficial skin changes (29,31).Using the backward mode, we found the remaining two predictor variables. The odd ratio was 0·111 for a fibre sheet, meaning that patient who uses a standard hospital sheet has a higher risk for the development of pressure ulcers and superficial skin changes. Thus, the combination of a proper support surface and a favourable bed sheet could effectively prevent pressure ulcers and superficial skin changes.

Subscale friction and shear scores were significant in the clinical setting. We found that subscale friction and shear scores for the group with pressure ulcers and superficial skin changes (1·2 ± 0·4) were significantly lower than those for the group with no skin changes (2·0 ± 0·2) ($P=0·000$). A management approach that considers friction and shear may involve using an appropriate technique for turning and repositioning the patient and using a favourable support surface sheet that can control the microclimate and reduce the coefficient of friction.

Study limitations

During the study, many participants dropped out as a result of medical conditions (such as getting worse, unable to turning lateral, pain), medical procedures (such as postoperative procedure, transferred to intensive care unit, haemodialysis schedule) or personal choice. Moreover, the limitation of time by the protocol of measurement between 8:00 AM and 12:00 AM made it possible to measure parameters in only 2–3 participants a day. High humidity (60–80%) and high temperature (±30°C) in the ward stimulated perspiration, making the measurement of skin moisture difficult. In addition, because of device problems, we only obtained interface pressure data from 33 participants, so that they were not entered in a stepwise-reduction of logistic regression analysis, which made us unable to evaluate the relationship between pressure ulcer development and interface pressure.

Implication in clinical practice

Our findings will be useful in a clinical setting because these measurements were not serial observations, meaning that the monitoring of skin temperature can be performed at one time point using a comparison with another site.

In our results, 45% of wounds were superficial skin changes and 47·8% were located in the lower sacrum (buttocks, intertriginous of gluteus). This finding reinforces the paradigm shift from a pressure ulcer problem to more widespread problems (superficial skin changes) and from bony prominence problems to whole buttock problems.

In addition, total skin temperature differences were marginally significant compared with the control site. Thus, skin temperature can be useful for detecting the early signs of any skin changes. This quantitative measurement is more reliable than a subjective evaluation and is also useful for patients with dark skin tone, in which the presence of erythema is sometimes difficult to evaluate. The evidence from this study suggests that skin temperature can be useful as a predictor measurement in order to establish preventive care.

Conclusion

Increasing skin temperature can be used as a quantitative measurement to predict the development of pressure ulcers and superficial skin changes and to evaluate support surface capability against microclimate factors. In addition, the use of a synthetic fibre sheet has the potential to control microclimate conditions between the patient's skin and support surface, which can reduce the development of pressure ulcers and other superficial skin changes. Finally, we can conclude that increasing skin temperature as a microclimate variable has a relationship with the development of pressure ulcers and superficial skin changes. Conversely, the type of bed sheet has a role in maintaining a favourable microclimate to prevent skin changes.

Acknowledgements

All synthetic fibre sheets were provided by Cape, Kanagawa, Japan. The company had no role in the study design, methods, subject recruitments, data collection, analysis and manuscript preparation.

References

1. Vanderwee K, Clark M, Dealey C, Gunningberg L, Defloor T. Pressure ulcer prevalence in Europe: a pilot study. *J Eval Clin Pract* 2007;**13**:227–35.
2. National Pressure Ulcer Advisory Panel and European Pressure Ulcer Advisory Panel. *Prevention and treatment of pressure ulcers: clinical practice guideline*. Washington DC: National Pressure Ulcer Advisory Panel, 2009.
3. Suriadi, Sanada H, Sugama J, Thigpen B, Subuh M. Development of a new risk assessment scale for predicting pressure ulcers in an intensive care unit. *Nurs Crit Care* 2008;**13**:34–43.
4. Kwong EW, Pang SM, Aboo GH, Law SS. Pressure ulcer development in older residents in nursing homes: influencing factors. *J Adv Nurs* 2009;**65**:2608–20.
5. Sanada H, Miyachi Y, Ohura T, Moriguchi T, Tokunaga K, Shido K, Nakagami G. The Japanese pressure ulcer surveillance study: a retrospective cohort study to determine prevalence of pressure ulcers in Japanese hospitals. *Wound* 2008;**2**:176–82.
6. Bergstrom N, Braden BJ, Laguzza A, Holman V. The Braden Scale for predicting pressure sore risk. *Nurs Res* 1987;**36**:205–10.
7. Gefen A. How do microclimate factors affect the risk for superficial pressure ulcers: a mathematical modeling study. *J Tissue Viability* 2011;**20**:81–8.
8. Sibbald RG, Krasner DL, Woo KY. Pressure ulcer staging revisited: superficial skin changes & deep pressure ulcer framework. *Adv Skin Wound Care* 2011;**24**:571–80.
9. Wounds International. *International review. Pressure ulcer prevention: pressure, shear, friction and microclimate in context. A consensus document*. London: Wounds International, 2010.
10. Clark M, Black J. Skin IQ^{TM} microclimate made easy. *Wounds Int* 2011;**2**:1–6.
11. Baldwin KM. Transcutaneous oximetry and skin surface temperature as objective measures of pressure ulcer risk. *Adv Skin Wound Care* 2001;**14**:26–31.
12. Sprigle S, Linden M, McKenne D, Davis K, Riordan B. Skin temperature measurement to predict incipient pressure ulcers. *Adv Skin Wound Care* 2001;**14**:133–7.
13. Hershler C, Conine TA, Nunn A, Hannay M. Assessment of an infrared non-contact Sensor for routine skin temperature monitoring: a preliminary study. *J Med Eng Technol* 1992;**16**:117–22.
14. Rapp MP, Bergstrom N, Padhye NS. Contribution of skin temperature regularity to the risk of developing pressure ulcers in nursing facility residents. *Adv Skin Wound Care* 2009;**22**:506–13.
15. Wong VK, Stotts NA, Hopf HW, Dowling GA, Froelicher ES. Changes in heel skin temperature under pressure in hip surgery patients. *Adv Skin Wound Care* 2011;**24**:562–70.
16. Knox DM. Core body temperature, skin temperature, and interface pressure. Relationship to skin integrity in nursing home residents. *Adv Wound Care* 1999;**12**:246–52.
17. Lavery LA, Higgins KR, Lanctot DR, Constantinides GP, Zamorano RG, Armstrong DG, Athanasiou KA, Agrawal CM. Home monitoring of foot skin temperatures to prevent ulceration. *Diabetes Care* 2004;**27**:2642–7.
18. Armstrong DG, Holtz-Neiderer K, Wendel C, Mohler MJ, Kimbriel HR, Lavery LA. Skin temperature monitoring reduces the risk for diabetes foot ucleration in high-risk patients. *Am J Med* 2007;**120**:1042–6.
19. Armstrong DG, Lavery LA, Liswood PJ, Todd WF, Tredwell JA. Infrared dermal thermometry for the high-risk diabetic foot. *Phys Ther* 1997;**77**:169–75.
20. Kelechi TJ, Haight BK, Herman J, Michel Y, Brothers T, Edlund B. Skin temperature and chronic venous insufficiency. *J Wound Ostomy Continence Nurs* 2003;**30**:17–24.
21. Sayre EK, Kelechi TJ, Neal D. Sudden increase in skin temperature predicts venous ulcers: a case study. *J Vasc Nurs* 2007;**25**:46–50.
22. Kelechi TJ, Michel Y. A descriptive study of skin temperature, tissue perfusion, and tissue oxygen in patients with chronic venous disease. *Biol Res Nurs* 2007;**9**:70–80.
23. Kokate JY, Leland KJ, Held AM, Hansen GL, Kveen GL, Johnson BA, Wilke MS, Sparrow EM, Iaizzo PA. Temperature-modulated pressure ulcers: a porcine model. *Arch Phys Med Rehabil* 1995;**76**:666–73.
24. Sae-Sia W, Wipke-Tevis DD, Williams DA. Elevated sacral skin temperature (Ts): a risk factor for pressure ulcer development in hospitalized neurologically impaired Thai patients. *Appl Nurs Res* 2005;**18**:29–35.
25. Bates-Jensen BM, McCreath HE, Pongquan V. Subepidermal moisture is associated with early pressure ulcer damage in nursing home residents with dark skin tones: pilot findings. *J Wound Ostomy Continence Nurs* 2009;**36**:277–84.
26. Newman DK, Preston AM, Salazar S. Moisture control, urinary and fecal incontinence, and perineal skin management. In: Krasner DL,

Rodeheaver GT, Sibbald RG, editors. *Chronic wound care: a clinical source book for healthcare professionals, 4th edn.* Malvern: HMP Communications, 2007:609–27.
27. Reger SI, Ranganathan VK, Sahgal V. Support surface, interface pressure, microenvironment and the prevalence of pressure ulcer: analysis of the literature. *Ostomy Wound Manage* 2007;**53**:50–8.
28. Gerhardt LC, Strassle V, Lenz A, Spencer ND, Derler S. Influence of epidermal hydration on the friction of human skin against textiles. *J R Soc Interface* 2008;**5**:1317–28.
29. Zhong W, Xing MMQ, Pan N, Maibach HI. Textiles and human skin, microclimate, cutaneous reactions: an overview. *Cutan Ocul Toxicol* 2006;**25**:23–39.
30. Nicholson GP, Scales JT, Clark RP, Calcina-Goff ML. A method for determining the heat transfer and water vapour permeability of patient support systems. *Med Eng Phys* 1999;**21**:701–12.
31. Zhong W, Ahmad A, Xing MM, Yamada P, Hamel C. Impact of textiles on formation and prevention of skin lesions and bedsores. *Cutan Ocul Toxicol* 2008;**27**:21–8.
32. Okamoto K, Kudoh Y, Yokoya T, Okudaira N. A survey of bedroom and bed climate of the elderly in a nursing home. *Appl Human Sci* 1998;**17**:115–20.
33. Jonsson A, Linden M, Lindgren M, Malmqvist LA, Backlund Y. Evaluation of antidecubitus mattresses. *Med Biol Eng Comput* 2005;**43**:541–7.
34. Patel S, Knapp CF, Donofrio JC, Salcido R. Temperature effects on surface pressure-induced changes in rat skin perfusion: implications in pressure ulcer development. *J Rehabil Res Dev* 1999;**36**:189–201.
35. Pell MF, Hirose H, Nicholson G, Call E. Thermodynamic rigid cushion loading indenter: a buttock-shaped temperature and humidity measurement system for cushioning surfaces under anatomical compression conditions. *J Rehabil Res Dev* 2009;**46**:945–56.
36. Min K, Son Y, Kim C, Lee Y, Hong K. Heat and moisture transfer from skin to environment through fabrics: a mathematical model. *Int J Heat Mass Transfer* 2007;**50**:5292–304.
37. VanGilder C, Amlung S, Harrison P, Meyer S. Results of the 2008–2009 International pressure ulcer prevalence survey and 3-year, acute care, unit-specific analysis. *Ostomy Wound Manage* 2009;**55**:39–45.
38. Bouten CVC, Knight MM, Lee DA, Bader DL. Compressive deformation and damage of muscle cell sub-populations in a model systems. *Ann Biomed Eng* 2001;**29**:153–63.
39. Kottner J, Halfens R. Moisture lesion: interrater agreement and reliability. *J Clin Nurs* 2010;**19**:716–20.
40. Beeckman D, Schoonhoven L, Fletche J, Furtado K, Gunningberg L, Heyman H, Lindholm C, Paquay L, Defloor T. EPUAP Classification system for pressure ulcer: European reliability study. *J Adv Nurs* 2007;**60**:682–91.
41. Doughty D. Differential assessment of trunk wounds: pressure ulceration versus incontinence associated dermatitis versus intertriginous dermatitis. *Ostomy Wound Manage* 2012;**58**:20–2.
42. Zulkowski K. Diagnosing and treating moisture-associated skin damage. *Adv Skin Wound Care* 2012;**25**:231–6.
43. Mahoney M, Rozenboom B, Doughty D, Smith H. Issue related to accurate classification of buttocks wounds. *J Wound Ostomy Continence Nurs* 2011;**38**:635–42.
44. Suriadi, Sanada H, Sugama J, Thigpen B, Kitagawa A, Kinoshita S, Murayama S. A new instrument for predicting pressure ulcer risk in an intensive care unit. *J Tissue Viability Soc* 2006;**16**:21–6.
45. Clarys P, Clijsen R, Taeymans J, Barel AO. Hydration measurements of the stratum corneum: comparison between the capacitance method (digital version of the Corneometer CM 825®) and the impedance method (Skicon-200EX®). *Skin Res Technol* 2012;**18**:316–23.
46. Guihan M, Bates-Jensen BM, Chun S, Parachuri R, Chin AS, McCreath H. Assessing the feasibility of sub epidermal moisture to predict erythema and stage 1 pressure ulcers in person with spinal cord injury: a pilot study. *J Spinal Cord Med* 2012;**35**:46–52.
47. Derler S, Rao A, Ballistreri P, Sailer AS, Rossi M. Medical textiles with low friction for decubitus prevention. *Tribol Int* 2011;**46**:208–14.
48. Gerhardt LC, Mattle N, Schrade GU, Spencer ND, Derler S. Study of skin–fabric interactions of relevance to decubitus: friction and contact-pressure measurements. *Skin Res Technol* 2008;**14**:77–88.
49. Pryczynska E, Symonowicz BL, Wieczorek A, Krekora K, Czapinska EB. Sheet fabrics with biophysical properties as elements of joint prevention in connection with first- and second-generation pneumatic anti-bedsore mattress. *Fibres Text East Eur* 2003;**11**:50–3.

OPEN ACCESS Freely available online

PLOS | ONE

Biological Responses of Three-Dimensional Cultured Fibroblasts by Sustained Compressive Loading Include Apoptosis and Survival Activity

Toshiki Kanazawa[1], Gojiro Nakagami[1], Takeo Minematsu[1], Takumi Yamane[1,2], Lijuan Huang[1], Yuko Mugita[1], Hiroshi Noguchi[3], Taketoshi Mori[3], Hiromi Sanada[1]*

1 Department of Gerontological Nursing/Wound Care Management, Graduate School of Medicine, The University of Tokyo, Tokyo, Japan, **2** Department of Nutritional Sciences, Faculty of Applied Bioscience, Tokyo University of Agriculture, Tokyo, Japan, **3** Department of Life Support Technology, Graduate School of Medicine, The University of Tokyo, Tokyo, Japan

Abstract

Pressure ulcers are characterized by chronicity, which results in delayed wound healing due to pressure. Early intervention for preventing delayed healing due to pressure requires a prediction method. However, no study has reported the prediction of delayed healing due to pressure. Therefore, this study focused on biological response-based molecular markers for the establishment of an assessment technology to predict delayed healing due to pressure. We tested the hypothesis that sustained compressive loading applied to three dimensional cultured fibroblasts leads to upregulation of heat shock proteins (HSPs), CD44, hyaluronan synthase 2 (HAS2), and cyclooxygenase 2 (COX2) along with apoptosis *via* disruption of adhesion. First, sustained compressive loading was applied to fibroblast-seeded collagen sponges. Following this, collagen sponge samples and culture supernatants were collected for apoptosis and proliferation assays, gene expression analysis, immunocytochemistry, and quantification of secreted substances induced by upregulation of mRNA and protein level. Compared to the control, the compressed samples demonstrated that apoptosis was induced in a time- and load- dependent manner; vinculin and stress fiber were scarce; HSP90α, CD44, HAS2, and COX2 expression was upregulated; and the concentrations of HSP90α, hyaluronan (HA), and prostaglandin E_2 (PGE_2) were increased. In addition, the gene expression of antiapoptotic *Bcl2* was significantly increased in the compressed samples compared to the control. These results suggest that compressive loading induces not only apoptosis but also survival activity. These observations support that HSP90α, HA, and, PGE_2 could be potential molecular markers for prediction of delayed wound healing due to pressure.

Citation: Kanazawa T, Nakagami G, Minematsu T, Yamane T, Huang L, et al. (2014) Biological Responses of Three-Dimensional Cultured Fibroblasts by Sustained Compressive Loading Include Apoptosis and Survival Activity. PLoS ONE 9(8): e104676. doi:10.1371/journal.pone.0104676

Editor: Johanna M. Brandner, University Hospital Hamburg-Eppendorf, Germany

Received January 17, 2014; **Accepted** July 16, 2014; **Published** August 7, 2014

Funding: This work was supported by a Grant-in-Aid for Scientific Research (A) from JSPS (Japan Society for the Promotion of Science) (No. 23249088). JSPS had no role in study design, data collection and analysis, decision to publish, or preparation of the manuscript.

Competing Interests: The authors have declared that no competing interests exist.

* Email: hsanada-tky@umin.ac.jp

Introduction

A recent study indicates that the prevalence of pressure ulcer (PU) is 13.7% in all care settings, including acute, long-term, rehabilitation, and home care settings [1]. This unacceptably high prevalence may be related to its chronicity, representing delayed wound healing due to pressure, which mainly inhibits tissue granulation in the wound healing process. A PU is continuously exposed to pressure as noted in its definition that PU is a localized damage to the skin and the underlying tissue, mainly caused by continuous exposure to pressure [2]. This is particularly true in immobile elderly and spinal cord injury patients; thus, it is quite difficult to completely eliminate pressure.

Early intervention for preventing delayed healing of PUs due to pressure requires a prediction method. Although clinical manifestations such as "thickened edges" [3] and "double erythema" [4] have been reported, they only indicate that pressure has already affected the PU healing process and do not help determine an appropriate preventive strategy for detection. To our knowledge, although some studies about delayed wound healing related with malnutrition or infection has reported [5], no study has reported the prediction of delayed wound healing due to pressure.

Why is no method available for predicting delayed healing due to pressure? This could be due to 2 reasons. First, it is quite difficult to estimate pressure-induced mechanical stress within the tissue, which directly causes cell damage and is measured using a pressure sensor such as a multi-pad type device that is widely used in clinical practice [6]. Second, we cannot estimate the magnitude of mechanical stress responsible for cell damage. Even if mechanical stress can be measured, the cellular response that leads to tissue damage is not uniform because of interpatient variability related to comorbidity, wound location, nutrition, and age [5,7 9]. We therefore considered that analysis of the cellular response to mechanical stress is the best approach for the prediction of delayed wound healing due to pressure. To investigate the cellular response, it is very important to reveal the molecular-level phenomena within the cell that lead to cell

damage; thus, an *in vitro* model would be the most suitable option for this purpose.

In the present study, we focused on the biological response-based molecular markers for the establishment of an effective assessment technology to predict delayed wound healing due to pressure. Specifically, we investigated the changes in gene expression by applying sustained compressive loading to the fibroblasts in a collagen sponge, which mimics the situation when pressure is continuously applied to the granulation tissue filled with fibroblasts and extracellular matrix (ECM). We subsequently identified the secreted substance along with gene expression as a molecular marker that could be collected noninvasively from the wound exudates in a clinical setting. Moseley et al. [8] reported in their review that analysis of wound exudates has a scientific and objective rationale for assessing the wound condition.

Although there are few studies that applied sustained compressive loading to the fibroblasts under three-dimensional (3D) culture for this purpose, in exploring the molecular markers we decided to investigate the gene expression of *heat shock proteins* (*Hsps*), *Cd44*, *hyaluronan synthase 2* (*Has2*), and *cyclooxygenase 2* (*Cox2*) as key factors related with mechanical stress and apoptosis [10–17]. In addition, our study focused on apoptotic cell death triggered by loss of ECM contacts, which indicates disruption of cell adhesion [13,14,18]. Previous studies have reported that increased apoptosis within the granulation tissue may contribute to impaired wound healing [19], and mechanical stress may induce apoptosis via disruption of adhesion [20,21], which leads to the idea that compression induces apoptosis triggered by the disruption of adhesion.

To test the hypothesis that sustained compressive loading applied to 3D cultured fibroblasts leads to upregulation of HSPs, CD44, HAS2, and COX2 along with apoptosis *via* disruption of adhesion, we applied sustained compressive loading to fibroblast-seeded collagen sponges.

Materials and Methods

Cell culture

The rat fibroblast cell line Rat-1 (RIKEN BioResource Center, Ibaraki, Japan) was grown at 37°C under 5% CO_2 in DMEM (Nacalai Tesque, Kyoto, Japan) supplemented with 10% FBS (Biowest, Nuaillé, France) and antibiotics (100 U/ml penicillin, 100 μg/ml streptomycin; Nacalai Tesque), and then cultured in a monolayer.

Cell seeding to the collagen scaffold

A porous atelocollagen sponge (MIGHTY; KOKEN, Tokyo, Japan) was used as a scaffold. The pore size was designed to be 100 200 μm, and the pores were interconnected. Trypsinized cells (2.0×10^7/pellet) collected by centrifugal force were suspended in 2.4 ml of 0.5% atelocollagen solution (KOKEN) supplemented with 0.3 ml of 10× concentrated DMEM prepared by dissolving DMEM powder (Biological Industries, Beit Haemek, Israel) in sterilized distilled water and 0.3 ml reconstitution buffer (Nitta Gelatin, Osaka, Japan) on ice to produce a cell suspension in a 0.4% collagen solution of DMEM. In total, 100 μl of cell suspension was seeded onto a collagen scaffold (5-mm diameter, 3-mm thick) by centrifugation (500×*g*, 5 min).

Compressive loading and loading protocol

Collagen sponge samples were precultured for 24 h and subjected to sustained compressive loading under 5% CO_2 at 37°C by using a custom-built loading apparatus (Fig. 1). The loading apparatus applied compression to the samples in a 12-well plate with stainless steel indenters, using a 5-mm thick stainless steel plate on top of the 12-well plate to stabilize the indenter. Various weights can be placed on top of these indenters to apply specified compression to the samples. Pressures of 0, 50, 100, or 200 mmHg, by following the report of Swain [22], were applied on samples for 2, 4, or 6 h. The sample with no treatment (0 h 0 mmHg) was analyzed as the baseline. Experiments were repeated 5 times.

WST-1 assay

Proliferative activity of fibroblasts was analyzed using the colorimetric WST-1 assay (Roche Diagnostics, Basel, Switzerland). In brief, collagen sponge samples after loading were transferred to new 12-well plates in 1 ml of medium containing 100 μl WST-1 reagent per well and then incubated for 1.5 h. The absorbance at 450 nm was measured using a microplate reader, DTX800 (Beckman Coulter, Brea, CA). The proliferative activity of each sample was shown as a relative value of absorbance compared to the baseline sample.

The terminal deoxy-nucleotidyl transferase-mediated deoxyuridine triphosphate nick end-labeling (TUNEL) staining

Quantification of apoptosis was measured using the *In situ* Apoptosis Detection Kit (TAKARA Bio Inc., Shiga, Japan). One

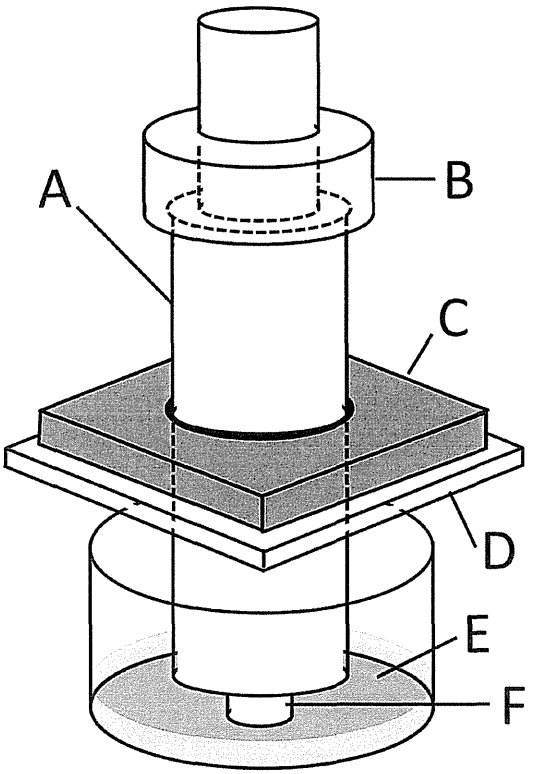

Figure 1. Loading apparatus to apply sustained compressive loading to cells seeded-collagen sponge. In this representation A indicates an indenter (diameter: 10 mm), B the weights, C a stainless steel plate (thick: 5 mm), D a 12-well plate lid, E culture medium, and F a fibroblast-seeded collagen sponge sample (diameter: 5 mm and thick: 3 mm).
doi:10.1371/journal.pone.0104676.g001

side of each collagen sponge cut in half after the WST-1 assay was fixed in 4% paraformaldehyde in phosphate buffer, dehydrated with series of ethanol, cleansed with series of xylene and embedded in paraffin. Longitudinal 4-μm thick sections were deparaffinized. Following TUNEL staining performed according to the manufacturer's instruction, the nucleus was stained with DAPI. The stained cells were observed under an inverted fluorescence microscope (DMI4000B; Leica, Wetzlar, Germany). The number of TUNEL-positive cells was counted in 5 fields in the central area of the collagen sponge (magnification ×10), and the proportion of positive cells to total cells was calculated.

Morphology and immunocytochemistry

Longitudinal 5-μm thick sections of 3D cell culture were deparaffinized and hematoxylin and eosin (H&E) staining was performed.

Rhodamine phaloidin and vinculin staining was performed on 3D cell culture samples as follows. The sections were incubated with rhodamine phaloidin for 45 minutes at room temperature (100 nM in 1% BSA; Cytoskeleton, Denver, CO). For vinculin, the sections were incubated with anti-vinculin rabbit polyclonal antibody (Sigma-Aldrich, St. Louis, MO; diluted 1:100) for 60 min at room temperature after antigen retrieval (semi boiling for 10 min in 10 mM citrate buffer, pH 6.0). Subsequently, the sections were incubated with Dylight® 488 anti-rabbit IgG antibody (Vector Laboratories, Burlingame, CA; diluted 1:1000) for 30 min at room temperature. The nucleus was stained with DAPI in both stainings. Between each step, the sections were washed 3 times with PBS for 5 min each. The stained cells were observed under an inverted fluorescence microscope (DMI4000B).

HSP90α, CD44, and COX2 immunostaining was performed on 3D cell culture as follows: the sections were incubated with anti-HSP90α rabbit polyclonal antibody (Lab Vision Corporation, Fremont, CA), anti-HCAM rabbit polyclonal antibody (Santa Cruz Biotechnology, Dallas, TX), or anti-COX2 rabbit monoclonal antibody (Cell Signaling Technology, Danvers, MA) at room temperature for 60 min (each antibody was diluted 1:50) after quenching of endogenous peroxidase and antigen retrieval (3D cell culture samples were subjected to semi boiling for 10 min). Subsequently, the sections were incubated with biotin-conjugated anti-rabbit IgG antibody (Jackson ImmunoResearch Laboratories, West Grove, PA; diluted 1:1000) for 30 min at room temperature. Immunoreactions were detected using a VectaStain ABC Kit (Vector Laboratories) with 3,3′- diaminobenzidine tetrahydrochloride substrate (Nacalai Tesque) and counterstained using hematoxylin.

HAS2 immunostaining was performed with anti-HAS2 mouse monoclonal antibody as the primary antibody (Santa Cruz Biotechnology; diluted 1:50) and then, as the secondary antibody, HRP-conjugated anti-mouse IgG antibody (Bethyl Laboratories, Montgomery, TX; diluted 1:1000). Any other kind of immunostaining methods was performed as well as methods described above. The samples were observed using an upright microscope (BX41; Olympus, Tokyo, Japan).

RNA extraction and real-time reverse transcription-polymerase chain reaction (RT-PCR)

Total RNA was extracted from the fibroblasts seeded on a collagen sponge following standard procedures using the RNeasy Plus Mini Kit (QIAGEN, Hilden, Germany). The other side of each collagen sponge, cut in half after the WST-1 assay, was minced and homogenized in liquid nitrogen. cDNA synthesis was performed using the TM100™ Thermal Cycler (Bio-Rad, Richmond, CA) and the High Capacity cDNA Reverse Transcription Kit (Life Technologies, Carlsbad, CA). For quantitative PCR, amplification of the target-specific region of cDNA was performed using Power SYBR® Green PCR Master Mix (Life Technologies) in a real-time PCR system (Mx3000P QPCR System; Agilent Technologies, Santa Clara, CA). The PCR protocol was as follows: 40 cycles at 95°C for 30 s and 60°C for 1 min after preheating at 95°C for 10 min. The expression of the target genes in the 6 h 200 mmHg group relative to the value in the 6 h 0 mmHg group was calculated by the comparative Ct method using the 18S ribosomal RNA gene as an internal control. The primer sequences are shown in Table 1. We confirmed that WST-1 measurement did not affect the gene expression analysis.

ELISA

The culture medium was collected after compressive loading. HSP90α concentration was measured using the Rat Heat Shock Protein 90α ELISA kit (CUSABIO BIOTECH, Wuhan, China). The concentration of hyaluronan (HA) was measured using the QnE Hyaluronic Acid ELISA Assay (Biotech Trading Partners, Encinitas, CA). The concentration of prostaglandin E_2 (PGE_2) was measured using the PGE_2 high sensitivity EIA kit (Enzo Life Sciences, Farmingdale, NY). Each experiment was performed according to the manufacturer's instructions. The values were normalized based on the cell number measured with the value of the WST-1 assay.

Statistical analysis

The results have been presented as mean ± SEM value. Statistical differences between the 2 groups were determined using the Student's t-test. The differences among multiple groups were compared by Dunnett's method using the baseline or 0 mmHg group as the control. A p value <0.05 was considered statistically significant. The software IBM SPSS Statistics for Windows version 20.0 (IBM, Armonk, NY) was used for all statistical analyses.

Results

3. 1. Sustained compressive loading did not induce apparent cell proliferation and induced apoptosis through disruption of adhesion

WST-1 assay and TUNEL staining were used to investigate the proliferative and the apoptotic effects of sustained compressive loading at various loading times and intensities in 3D cultured fibroblasts. While the cell number in nonloaded groups significantly increased compared with the baseline in a time-dependent manner (2, 4, and 6 h groups; $p=0.872$, $=0.147$, and $=0.018$, respectively; Fig. 2A), such an increase over the baseline was not observed in 2, 4, and 6 h 200 mmHg groups (each group; $p>0.05$; Fig. 2B). Moreover, 6-h compressive loading induced a significant reduction in the cell number of the 50, 100, and 200 mmHg groups compared with the 0 mmHg group (each group; $p<0.01$; Fig. 2C). An increase in apoptosis was not observed in nonloaded groups (each group; $p>0.05$; Fig. 2D). In contrast, compressive loading significantly induced apoptosis in a time- and load-dependent manner (according to loading time for 2, 4, and 6 h 200 mmHg, $p=0.002$, <0.001, and <0.001, respectively; according to loading intensity at 6 h 50, 100, and 200 mmHg, $p<0.001$, <0.001, and <0.001, respectively; Fig. 2E and 2F). Although these results suggest that proliferation and apoptosis occur simultaneously during compressive loading, apparent cell proliferation did not occur. We thus considered this system as the inhibitory state of granulation.

The detachment of anchorage-dependent cells, such as fibroblasts, induces apoptosis which is called "anoikis" [23]. In the

Table 1. Primer sequences used for the quantification of gene expression.

Target gene	Primer sequeces (5′-3′)		GenBank
	Forward	Reverse	accession number
Hsf1	TTGACTCCATCCTTCGAGA	CCAGGTGATCACTTAGCTC	NM_024393.1
Hsf2	TCAGGAAGACAGTTTAGCAT	AAAGGCAGTGTACTGGATAA	NM_031694.2
Hsp32	AGTTCAAACAGCTCTATCGT	GTAGTATCTTGAACCAGGCT	NM_012580.2
Hsp40	GCGAGATTTTCGACCGCTAT	GATTCCTGCCACCGAAGAAC	NM_001108441.1
Hsp47	CTCGTTAATGCCATGTTCTT	TCTCGTCGTCATAGTAGTTG	NM_017173.1
Hsp60	TCGCCAGATGAGACCAGTGT	TGGGACTTCCCCAACTCTGT	NM_022229.2
Hspa5	CATTCAAGGTGGTTGAAAAG	TGCATCATTGAAGTAAGCTG	NM_013083.2
Hsc70	TGAGAATGTTCAGGATTTGC	CATACACCTGGATGAGTACA	NM_024351.2
Hsp90aa1	GTGCGGTTAGTCACGTT	TCGAGTAGAAAGTGTTGATG	NM_175761.2
Bcl2	GCGTCAACAGGGAGATGTCA	GCTGAGCAGCGTCTTCAGAG	NM_016993.1
Bax	GATGATTGCTGACGTGGACA	TGATCAGCTCGGGCACTTTA	NM_017059.2
Cd44	CCGTTACGCAGGTGTATTCC	TGTTGAAAGCCTCGCAGAG	NM_012924.2
Has1	TTCAAGGCACTGGGTGACTC	CCCAGTATCGAAGGCTGCTC	NM_172323.1
Has2	AGGGGACCTGGTGAGACAGA	GGGTCAAGCATGGTGTCTGA	NM_013153.1
Has3	GTGTTCGAGCTGTGGTGTGG	GGGGATCTTCCTCCAAGACC	NM_172319.1
Vcan	TGAATGTCACTCTAACCCTT	ATTGCCCTTGGAATTTGTG	NM_053663.1
Tnfaip6	GCTTTGTAGGAAGATACTGC	CCTTGATTGGATTTAGGTGC	NM_053382.1
Hyal1	CCTTCAGTCCTGAGGTTTCC	CCAGTGAGTGTCTGCATTCC	NM_207616.1
Hyal2	CAGAACTTAGCCAGATGGAC	CACATTGACTATGTAGGGGA	NM_172040.2
Hyal3	TCTTCCCTAGCATCTACCTC	TAGGTCATCCAGAGACAAGA	NM_207599.2
Mmp2	ACAGGACCCTGGAGCTTTGA	CTTGCAGATCTCGGGAGTGA	NM_031054.2
Mmp3	AAGATGCTGGCATGGAGGTT	TTCGAGTCCAGCTTCCCTGT	NM_133523.2
Mmp9	GCGCTGGGCTTAGATCATTC	TGGGACACATAGTGGGAGGA	NM_031055.1
Mmp13	ATGTGGAGTGCCTGATGTGG	GCCATCATGGATCCTGGTAAA	NM_133530.1
Cox2	CCCACTTCAAGGGAGTCTGG	GCAGTCATCAGCCACAGGAG	NM_017232.3

doi:10.1371/journal.pone.0104676.t001

process of anoikis, cell detachment from ECM induces apoptosis by disrupting survival signals generated through cytoskeletal rearrangements induced by cell integrin-ECM interactions, including the formation of focal adhesions (FAs) and actin filament stress fibers [18,24,25]. We therefore investigated the effects of sustained compressive loading on cell morphology, FA, and actin stress fiber formation in 3D cultured fibroblasts. First, we compared the cell morphology, identified by H&E staining, for the 6 h 0 mmHg and the 6 h 200 mmHg groups. The distinctive cell morphology observed in the 6 h 0 mmHg group was spindle-shaped cells, whereas that in the 6 h 200 mmHg group was nonspindle-shaped cells along with apoptotic bodies (Fig. 2G, 2H, and 2I). Second, we compared the expression of FAs, identified by staining of the FA structural protein vinculin, for the 6 h 0 mmHg and the 6 h 200 mmHg groups. Vinculin expression was observed in the 6 h 0 mmHg group, whereas it was scarcely observed in the 6 h 200 mmHg group (Fig. 2J and 2K). Similarly, actin stress fibers were observed in the 6 h 0 mmHg group, but not in the 6 h 200 mmHg (Fig. 2L and 2M). Thus, in the cells of 6 h 200 mmHg group without apoptotic bodies, vinculin and actin stress fibers were scarce even before the cells underwent apoptosis. The observation that vinculin and actin stress fibers were scarce even in cells without apoptotic bodies supports the proapoptotic effects of compressive loading on fibroblasts by disruption of adhesion.

Gene expression was compared between the 6 h 0 mmHg and the 6 h 200 mmHg groups to narrow down the candidates of the molecular markers because, by integrating the results of cell number and apoptosis, most differences would be observed between these 2 groups. After investigating gene expression, we measured the concentration of secreted substances in the cultured medium of the 0, 50, 100, and 200 mmHg groups to confirm the clinical applicability of markers for predicting tissue damage caused by the compressive loading.

Stress- and apoptosis-related gene expression was stimulated by 6-h compressive loading

A significant increase in the expression of *heat shock transcription factor 1* (*Hsf1*) and *Hsf2* was observed in the 200 mmHg group compared with the 0 mmHg group (*Hsf1* and *Hsf2*; $p = 0.006$ and $= 0.004$, respectively; Fig. 3A). Expression of these genes is induced by the disruption of adhesion [26], and HSF1 and HSF2 bind to the regulatory site of various *Hsp* genes. Following this, we investigated the influence of compressive loading on the gene expression of various HSPs, which are stress-responsive proteins against mechanical stress, elevated temperature, hypoxia, lowered pH, and reactive oxygen species (ROS) [27]. The expression of various *Hsps* was significantly higher in the 200 mmHg group than in the 0 mmHg group (*Hsp32*, *Hsp40*, *Hsp47*, *Hsp60*, *Hspa5*, *Hsc70*, and *Hsp90aa1*; $p = 0.002$, $= 0.019$, < 0.001, $= 0.024$, $= 0.033$, $<$

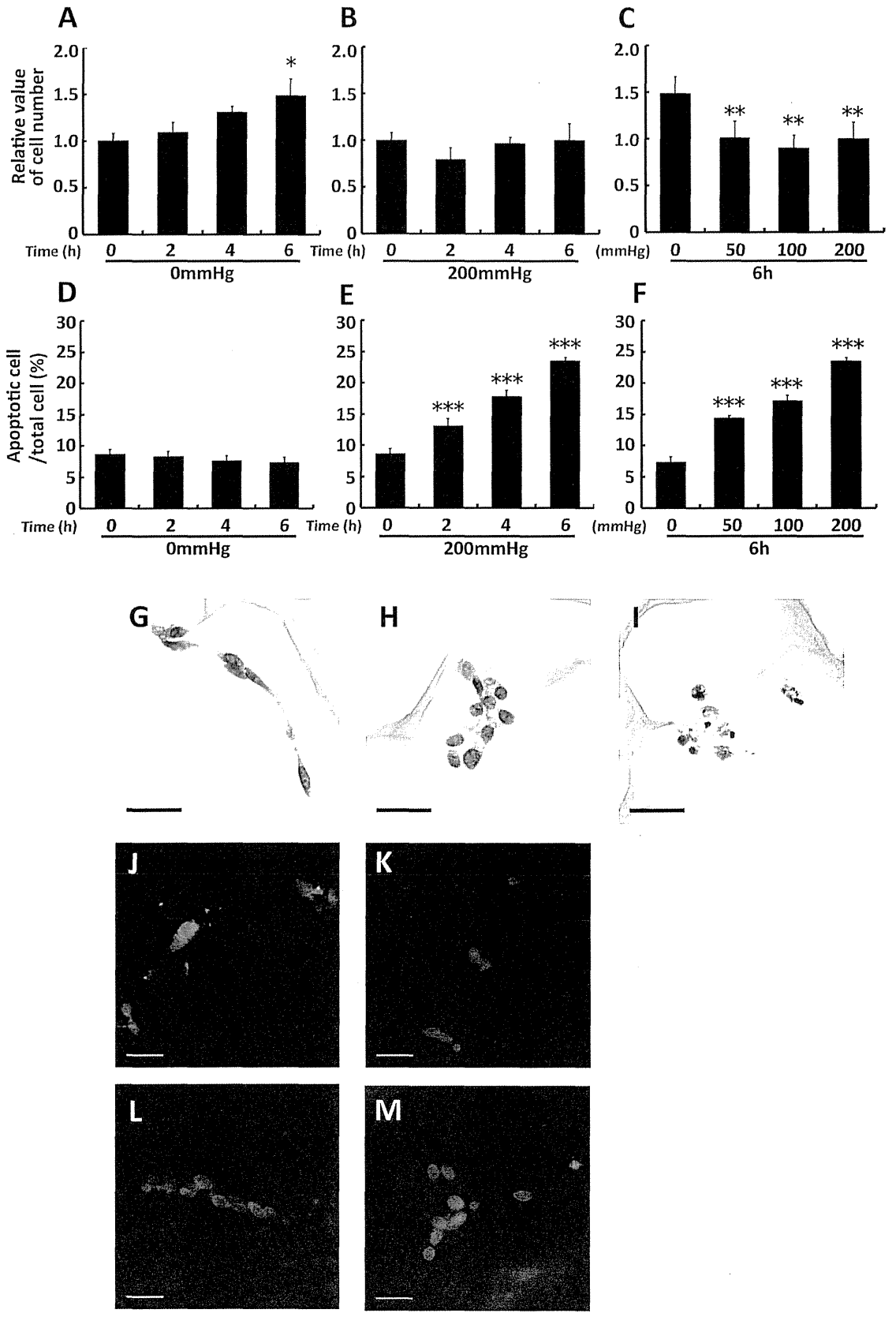
A
B
C
Relative value of cell number
2.0
1.5
1.0
0.5
0
*
Time (h) 0 2 4 6
0mmHg
Time (h) 0 2 4 6
200mmHg
(mmHg) 0 50 100 200
6h
**
D
E
F
Apoptotic cell /total cell (%)
30
25
20
15
10
5
***
G
H
I
J
K
L
M

Figure 2. Sustained compressive loading did not induce apparent cell proliferation and induced apoptosis through disruption of adhesion. Fibroblasts were seeded to collagen sponge and incubated for 24 h. And then they were subjected to 0, 50, 100, or 200 mmHg compression for 0, 2, 4, and 6 h. A, B, and C: Collagen sponge samples after loading were transferred to new 12-well plates in 1 ml medium containing 100 μl WST-1 reagent per well, and then incubated for 1.5 h. The absorbance of 450 nm was measured. The cell number was shown relative to base line. The results are represented as the mean ± SEM (error bars) of five experiments. D, E, and F: Collagen sponge samples were fixed, dehydrated, cleared, and processed for embedding in paraffin after loading experiments. Sections were prepared at 4-μm thick. Apoptosis assay were performed by TUNEL stain using tissue slides. The number of TUNEL-positive cells was counted in 5 fields in the central area of the collagen sponge (magnification ×10), and the proportion of positive cells to total cells was calculated. The results are represented as the mean ± SEM (error bars) of five experiments. Statistical analysis was performed using the Dunnett's multiple test: between 2, 4, or 6 h group and 0 h group (A, B, D, and E) or between each of loaded group and nonloaded group (C and F). Statistical significance was taken as $p<0.05$. A value of p was expressed as: *; $p<0.05$, **; $p<0.01$, and ***; $p<0.001$. G, H, and I: H&E staining for confirming cell morphology. Collagen sponge samples were prepared as aforementioned. Sections were prepared at 5-mm thick. The distinctive cell morphology observed in the 6 h–0 mmHg group was spindle-shaped cells (G), whereas that in the 6 h–200 mmHg group was nonspindle-shaped cells (H) along with apoptotic bodies (I). J and K: Immunostaining for the FA structural protein vinculin (green). Nucleus stained by DAPI (blue). Vinculin expression was observed in the 6 h–0 mmHg group (J), whereas it was scarcely observed in the 6 h–200 mmHg group (K). L and M: Immunostaining for actin stress fibers by phaloidin (red). Nucleus stained by DAPI (blue). Actin stress fibers were observed in the 6 h–0 mmHg group (L), but not in the 6 h–200 mmHg group (M). Scale bars = 20 μm for all images.
doi:10.1371/journal.pone.0104676.g002

0.001, and <0.001, respectively; Fig. 3B). Upregulation of various *Hsps* indicates that stress responses by compressive loading occurred in fibroblasts. To examine the condition of nonapoptotic cells, we investigated the expression of antiapoptotic *Bcl2* [28] and proapoptotic *Bax* [29]. The results indicated that *Bcl2* levels were significantly higher in the 200 mmHg group than in the 0 mmHg group, but *Bax* levels did not show any significant difference. ($p = 0.001$ and 0.851, respectively; Fig. 3C). Subsequently, we focused on HSP90α encoded by *Hsp90aa1* and investigated the expression of HSP90α by immunocytochemistry, because *Hsp32*, known as an oxidative stress marker, is upregulated by compressive loading and oxidative stress leads to the release of HSP90α into the extracellular environment [30,31]. Higher expression and nucleus translocation of HSP90α were observed in the 200 mmHg group when compared with the 0 mmHg group (Fig. 3D and 3E). Nucleus translocation of HSP90 occurs after cellular stress, and HSP90 tightly interacts with histones [32]. We decided to quantitatively evaluate HSP90α in the culture supernatants based on these observations.

Cd44, *Has2*, and *Cox2* were upregulated by 6-h compressive loading but HA binding proteins and hyaluronidase gene expression were not

A 9.0-fold increase occurred in *Cd44*, one of the adhesion molecules related to apoptosis *via* the disruption of adhesion [14], in the 200 mmHg group compared with the 0 mmHg group ($p<0.001$; Fig. 4A). Subsequently, we investigated *Has1*, *Has2*, and *Has3*, which are HA synthases, known as a primary ligand for CD44 [33 35]. A 4.6-fold increase occurred in *Has2* in the 200 mmHg group compared with the 0 mmHg group ($p<0.001$) (Fig. 4B). On the other hand, the levels of *Has1* and *Has3* were under the detection limit in both the groups. Subsequently, we investigated the expression of CD44 and HAS2 proteins by immunostaining because *Cd44* and *Has2* were significantly upregulated by compressive loading. Similar to gene expression, CD44 and HAS2 were upregulated by compressive loading in 3D cultured fibroblasts (Fig. 4C, 4D, 4E, and 4F). Based on these results, we decided to quantitatively evaluate HA synthesized by HAS2 in the culture supernatants. Furthermore, we investigated *Cox2* gene expression because CD44 and HA interaction upregulates COX2 expression [17]. *Cox2* was significantly upregulated by compressive loading ($p = 0.007$; Fig. 4G). Next, we investigated the expression of the COX2 protein by immunostaining based on the result for *Cox2* gene expression. Protein expression, as well as gene expression, for COX 2 was upregulated by compressive loading (Fig. 4H and 4I). Therefore, considering that PGE_2 is a secretory substance downstream of COX2 [36], PGE_2 would also be a possible molecular marker, that could be quantitatively evaluated in the culture supernatants.

In addition, for studying marker candidates besides HA and PGE_2, we investigated the expression of *versican (Vcan), tumor necrosis factor alpha-induced protein 6 (Tnfaip6), hyaluronidase 1 (Hyal1), Hyal2*, and *Hyal3*, considering that the expression of HA binding proteins and degrading enzyme was upregulated along with an increase in *Has2* expression. However, the results indicated the expression of *Vcan* and *Hyal1* was significantly lower in the 200 mmHg group than in the 0 mmHg group (*Vcan*, *Tnfaip6*, *Hyal1*, *Hyal2*, and *Hyal3*; $p = 0.003$, $= 0.290$, $= 0.045$, $= 0.088$, and $= 0.053$, respectively; Fig. 4J).

Secretions of HSP90α, HA and PGE_2 into the cell culture medium were increased by 6-h compressive loading

We then measured the concentration of HSP90α, HA, and PGE_2 in the culture medium. The concentration of HSP90α was significantly higher in the 50, 100, and 200 mmHg groups than in the 0 mmHg group ($p = 0.042$, $= 0.002$, and $= 0.004$, respectively; Fig. 5A). The concentration of HA was also significantly higher in the 100 and 200 mmHg groups than in the 0 mmHg group ($p = 0.014$ and $= 0.021$, respectively; Fig. 5B). On the other hand, the concentration of PGE_2 was significantly higher only in the 100 mmHg group than in the 0 mmHg group ($p = 0.004$). An increase in PGE_2 was observed in the 50 mmHg and the 200 mmHg groups compared with the 0 mmHg group ($p = 0.177$ and $= 0.149$, respectively; Fig. 5C) but this difference was not statistically significant.

Discussion

In the present study, we investigated candidates of molecular markers in order to predict delayed wound healing due to pressure focusing on cellular responses along with apoptosis triggered by the disruption of adhesion for the first time. Our results revealed that sustained compressive loading reduced the cell number and notably induced apoptosis in a time- and load-dependent manner. Furthermore, *Hsp90aa1*, *Cd44*, *Has2*, and *Cox2* were upregulated, and along with these upregulated genes, HSP90α, HA, and PGE_2 were also increased by sustained compressive loading in fibroblasts. We noted the possibility of developing an assessment technology to predict delayed wound healing due to pressure, based on gene and protein expression and substances related to gene and protein expression analysis.

Wang and Thampatty [37] have reviewed many studies on the altered gene expression related to compressive loading in different cell types such as osteoblasts, chondrocytes, synovial cells, and

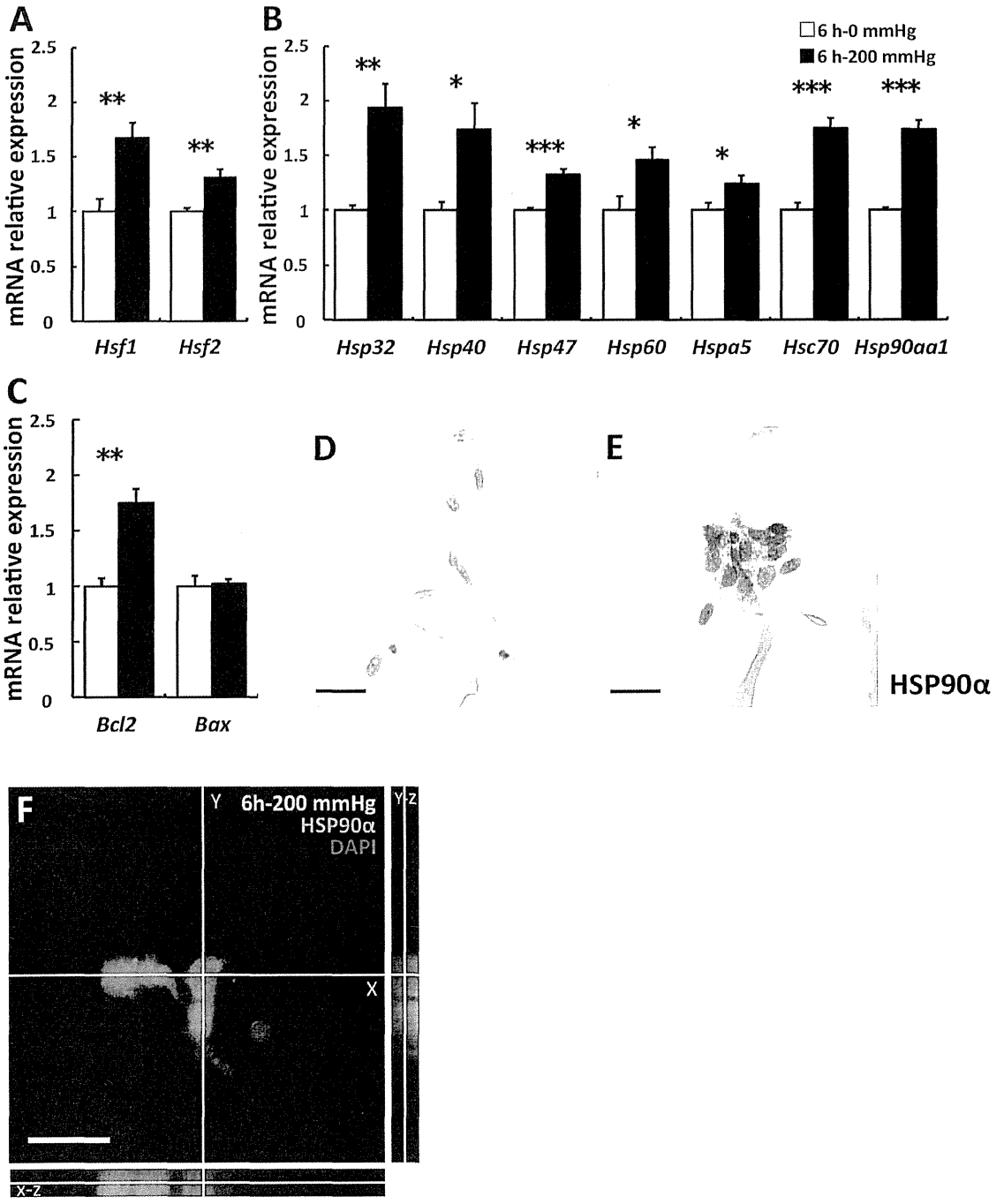

Figure 3. Stress- and apoptosis-related gene expression was stimulated by 6-h compressive loading. Fibroblasts were seeded to collagen sponge and incubated for 24 h. And then they were subjected to 0 mmHg (□) or 200 mmHg (■) compression for 6 h. Total mRNA was extracted after WST-1 assay, and mRNA expression was assessed using real-time RT-PCR. The expression of the target genes in the 6 h–200 mmHg group relative to the value in the 6 h–0 mmHg group was calculated by the comparative Ct method using the 18S ribosomal RNA gene as an internal control. The results are represented as the mean ± SEM (error bars) of five experiments. Statistical analysis was performed using the Student's t test between the 0 mmHg group and the 200 mmHg group, and statistical significance was taken as $p<0.05$. A value of p was expressed as: *; $p<0.05$, **; $p<0.01$, and ***; $p<0.001$. A: The transcription factors of various *Hsps*. B: various *Hsps* C: *Bcl2* is an antiapoptotic gene, and *Bax* is a proapoptotic gene. D and E: Immunostaining for HSP90α. Representative sections of (D) the 6 h–0 mmHg group and (E) the 6 h–200 mmHg group. Higher expression and nucleus translocation of HSP90α was observed in the 200 mmHg group (E) when compared with the 0 mmHg group (D). Scale bars = 20 μm for all images.

doi:10.1371/journal.pone.0104676.g003

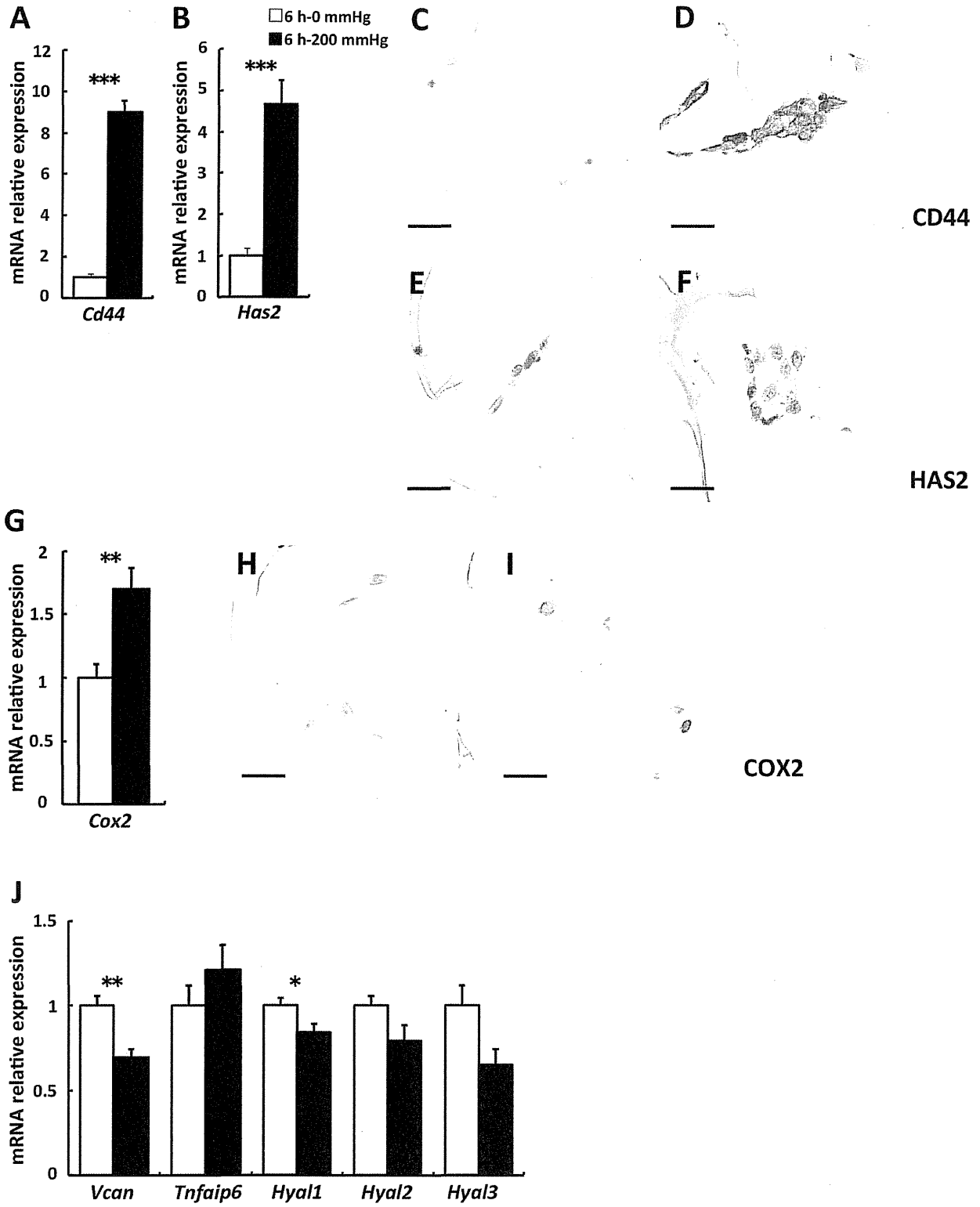

Figure 4. *Cd44* and *Has2* were upregulated by 6-h compressive loading, but HA binding proteins and hyaluronidase gene expression were not. Fibroblasts were seeded to collagen sponge and incubated for 24 h. And then they were subjected to 0 mmHg (□) or 200 mmHg (■) compression for 6 h. Total mRNA was extracted after WST-1 assay, and mRNA expression was assessed using real-time RT-PCR. The expression of the target genes in the 6 h–200 mmHg group relative to the value in the 6 h–0 mmHg group was calculated by the comparative Ct

method using the 18S ribosomal RNA gene as an internal control. The results are represented as the mean ± SEM (error bars) of five experiments. Statistical analysis was performed using the Student's t test between the 0 mmHg group and the 200 mmHg group, and statistical significance was taken as $p<0.05$. A value of p was expressed as: *; $p<0.05$, **; $p<0.01$, and ***; $p<0.001$. A: *Cd44*. B: *Has2*. G: *Cox2*. J: *Vcan* and *Tnfaip6* are HA binding proteins. *Hyal1*, *2*, and *3* are HA degrading enzyme. C and D: Immunostaining for CD44. Representative sections of (C) the 6 h–0 mmHg group and (D) the 6 h–200 mmHg group. E and F: Immunostaining for HAS2. Representative sections of (E) the 6 h–0 mmHg group and (F) the 6 h–200 mmHg group. H and I: Immunostaining for COX2. Representative sections of (H) the 6 h–0 mmHg group and (I) the 6 h–200 mmHg group. Scale bars = 20 μm for all images.
doi:10.1371/journal.pone.0104676.g004

periodontal ligament cells, which are exposed to compressive stimulation under physiological conditions. However, applying the previous results may not be appropriate for studying molecular markers induced by compressive stimulation in chronic wounds such as PUs because cellular responses are generally cell type dependent [37] and differs between sustained and cyclic manners for load application [15,21].

Our results suggest that sustained compressive loading induced apoptosis and did not support apparent cell proliferation. Therefore, we studied the available molecular markers using our experimental system. In this system, inhibition of granulation occurred along with apoptosis. Our purpose was to study the cellular responses leading to molecular markers in the cells, during apoptosis in 3D cultured fibroblasts, which mimics the granulation tissue. Our results also show that apoptotic cell rate in the 6 h 200 mmHg was over 3 times higher than in the 6 h 0 mmHg. Although our system is single cell model, our results represent the effect of apoptosis observed in our model on delayed wound healing due to pressure at least in part. In fact, there are some animal models of chronic wounds [38–41]. However, these animal models employed two magnetic plates to dorsal skin for making PUs [38,39] or treated with drugs to induce diabetic conditions before making full thickness wound [40,41] to create the chronic wounds, therefore cannot be used for assessing the effect of pressure applied to the existing wounds on its healing process.

We found that apoptosis was induced and *Hsps* expression was higher in the 200 mmHg group compared with the 0 mmHg group. This result is consistent with previous reports. Recent studies have demonstrated that HSPs are upregulated by mechanical stress in periodontal ligament cells and gastric mucosa cells [10–12] and that apoptosis is induced by mechanical stress [20,42,43]. Sreedhar and Csermely [26] reviewed that the upregulation of HSPs occurs during the induction of apoptosis reported in many studies. Hence, apoptosis, upregulation of HSPs, and mechanical stress are closely related.

The increase in *Hsps*, *Bcl2*, and *Bax* gene expression observed in our study suggests that nonapoptotic surviving cells promote survival activity. The present study demonstrates that compressive loading leads to various biological stresses, which induces apoptosis, because various *Hsps* were significantly increased in the loaded fibroblasts. Upregulation of *Hsp32* indicates that oxidative stress is generated [44]. *Hsp47* and *Hspa5* are expressed during the stress in the endoplasmic reticulum [26,45]. *Hsp60*, *Hsc70*, and *Hsp90aa1* encode chaperone proteins that repair damaged proteins and promote cell survival [26]. In addition, a correlation exists between ROS generation and the induction of HSPs [46], and the upregulation of BCL2 prevents mitochondrial ROS generation [47].

We observed remarkable upregulation of CD44 at both mRNA and protein levels by compressive loading. Upregulation of CD44 contributes to survival signals and promotes the resistance of apoptosis triggered by the disruption of adhesion [14,48,49]. Therefore, it is suggested that the induction of apoptosis in the present study has been caused by compression-induced disruption of adhesion.

The present study demonstrated that compressive loading increases the expression of HAS2 and that HA levels increase in fibroblasts. HAS2 synthesizes high molecular weight HA [50], which serves as a structural scaffold in the tissue [51]. HA has been shown to alter the physical properties of ECM [52], including hydration [53], diffusion [54], and viscoelasticity [55,56]. HA associated with proteoglycan anchors to the cell surface *via* CD44 in the pericellular matrix [57]. HA also holds aggregates of proteoglycan [58] and forms huge complexes that provide a load-bearing function in ECM [59]. Increased HA in this system may therefore improve load-bearing function and scaffold for cellular

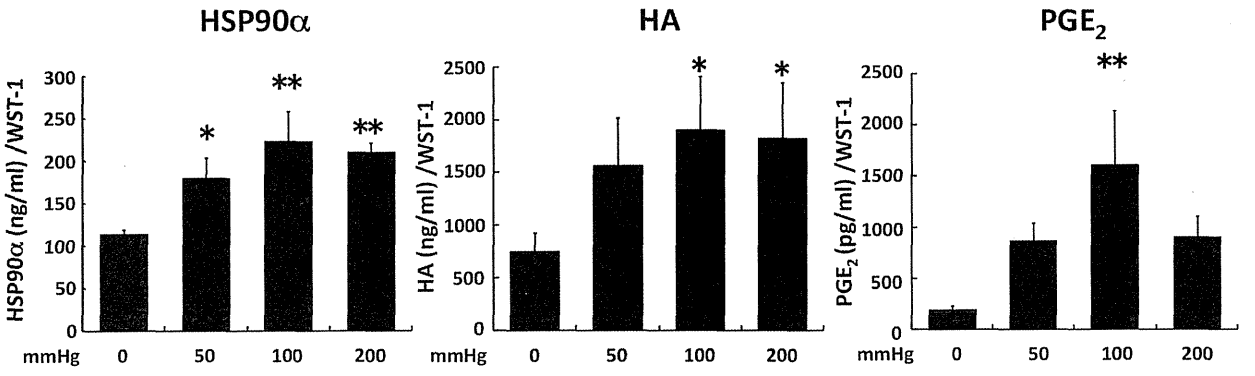

Figure 5. The secretions of HSP90α, HA, and PGE_2 into cell culture medium were increased by compressive loading. Fibroblasts were seeded to collagen sponge and incubated for 24 h. And then they were subjected to 0, 50, 100, or 200 mmHg compression for 6 h. Culture supernatants were collected after 6 h loading experiments. The level of each substance (A: HSP90α, B: HA, C: PGE_2) was measured by ELISA. A value of concentration was normalized by WST-1 value. The results are represented as the mean ± SEM (error bars) of five experiments. Statistical analysis was performed using the Dunnett's multiple test between non-loaded group and each of loaded group, and statistical significance was taken as $p<0.05$. A value of p was expressed as: *; $p<0.05$, **; $p<0.01$, and ***; $p<0.001$.
doi:10.1371/journal.pone.0104676.g005

adhesion. Takemura et al. [16] have reported that because of the elastic and hydrational properties of HA, an increase in HA by applying cyclic tensile stress to uterine cervical fibroblasts results in flexibility required during delivery. However, while upregulation of *Has2* and *Cd44* was observed by compressive loading, downregulation of *Vcan,* which encodes a core protein of proteoglycan, was also observed. Thus, it may not be sufficient to improve the load-bearing function and scaffold under sustained compressive loading. In previous study using tensile loading, Crockett et al. [15] have reported that the secretion of HA is increased in tendon fibroblasts, whereas the secretion of glycosaminoglycan becoming proteoglycan along with the core protein is not increased. This result is consistent with our result; however, in arterial smooth muscle cells using mechanical strain, the expression of protein and mRNA levels in versican was increased [60]. The difference in these results may occur as a result of the difference in the intensity and type of mechanical stress and cell type.

The present study also revealed upregulation of COX2 and PGE_2 by compressive loading. Although an increase in PGE_2 was observed in the 50 mmHg and the 200 mmHg groups when compared with the 0 mmHg group, a significant increase in PGE_2 was observed only in the 100 mmHg group. Our observation that an increase in PGE_2 does not occur in a load-dependent manner may suggest suppression of *Cox2* expression in the 200 mmHg group relative to that in the 100 mmHg group. As Misra et al. [17] have reported that fragmented HA suppresses *Cox2* expression, it is likely that HA was fragmented by ROS [61] in the 200 mmHg group and subsequently suppressed Cox2 expression. However, in our study the effect of compressive loading on the interaction of CD44 and HA and the occurrence of HA fragmentation has not been elucidated. Further studies are needed to establish these mechanisms.

The cellular responses reported here can be measured from the wound exudate because these factors are available in culture supernatants. Wound exudates may represent useful biomarkers in predicting the wound healing condition [8]. Furthermore, quantification of these markers using wound blotting [62] that has been developed in our laboratory would be applicable to a clinical setting.

We need to verify whether phenomena similar to those observed in our study also occur *in vivo* in animal experiments and in clinical patients. In this study, we investigated the *in vitro* cellular response of only 1 cell type, fibroblasts. The interaction of fibroblasts and inflammatory cells such as neutrophils and macrophages may alter cellular responses. Although our results show gene expression immediately after 6-h compressive loading, the expression change after release or repeated loading is unknown. Further studies are required to measure the concentration of matrix metalloproteinases, versican, HYAL1, and other factors, to improve the specificity of the assessment technology.

In this study, we investigated the cellular responses along with apoptosis triggered by sustained compressive loading-induced disruption of adhesion to predict delayed wound healing due to pressure. The results for the compressed samples demonstrated that apoptosis was induced in a load- and time-dependent manner; that *Hsp90aa1*, *Cd44*, *Has2*, and *Cox2* expression was upregulated; and that the concentrations of HSP90α, HA, and PGE_2 increased in the culture medium. Therefore, we have newly introduced these candidate molecular markers for establishing a prediction method for delayed wound healing due to pressure.

Author Contributions

Conceived and designed the experiments: TK GN T. Minematsu HS. Performed the experiments: TK GN T. Minematsu TY LH. Analyzed the data: TK GN T. Minematsu. Contributed reagents/materials/analysis tools: TK GN T. Minematsu TY LH YM HN T. Mori. Wrote the paper: TK GN.

References

1. VanGilder C, MacFarlane G, Meyer S, Lachenbruch C (2009) Body mass index, weight, and pressure ulcer prevalence: an analysis of the 2006–2007 International Pressure Ulcer Prevalence Surveys. J Nurs Care Qual 24: 127–135.
2. European Pressure Ulcer Advisory Panel and National Pressure Ulcer Advisory Panel (2009) Prevention and treatment of pressure ulcers: clinical practice guideline. Washington DC: National Pressure Ulcer Advisory Panel. 130 p.
3. Okuwa M, Sugama J, Sanada H, Konya C, Kitagawa A (2005) Measuring the pressure applied to the skin surrounding pressure ulcers while patients are nursed in the 30 degree position. J Tissue Viability 15: 3–8.
4. Sato M, Sanada H, Konya C, Sugama J, Nakagami G (2006) Prognosis of stage I pressure ulcers and related factors. Int Wound J 3: 355–362.
5. Wild T, Rahbarnia A, Kellner M, Sobotka L, Eberlein T (2010) Basics in nutrition and wound healing. Nutrition 26: 862–866.
6. Sugama J, Sanada H, Takahashi M (2002) Reliability and validity of a multi-pad pressure evaluator for pressure ulcer management. J Tissue Viability 2: 148–153.
7. Verzijl N, DeGroot J, Thorpe SR, Bank RA, Shaw JN, et al. (2000) Effect of collagen turnover on the accumulation of advanced glycation end products. J Biol Chem 275: 39027–39031.
8. Moseley R, Stewart JE, Stephens P, Waddington RJ, Thomas DW (2004) Extracellular matrix metabolites as potential biomarkers of disease activity in wound fluid: lessons learned from other inflammatory diseases? Br J Dermatol 150: 401–413.
9. Sae-Sia W, Wipke-Tevis DD, Williams DA (2007) The effect of clinically relevant pressure duration on sacral skin blood flow and temperature in patients after acute spinal cord injury. Arch Phys Med Rehabil 88: 1673–1680.
10. de Araujo RM, Oba Y, Moriyama K (2007) Identification of genes related to mechanical stress in human periodontal ligament cells using microarray analysis. J Periodontal Res 42: 15–22.
11. Odashima M, Otaka M, Matsuhashi T, Jin M, Horikawa Y, et al. (2007) Mechanical strain stress suppresses expression of HSP70 and wound restoration in gastric mucosal cells. Dig Dis Sci 52: 3087–3091.
12. Mitsuhashi M, Yamaguchi M, Kojima T, Nakajima R, Kasai K (2011) Effects of HSP70 on the compression force-induced TNF-α and RANKL expression in human periodontal ligament cells. Inflamm Res 60: 187–194.
13. Henke C, Bitterman P, Roongta U, Ingbar D, Polunovsky V (1996) Induction of fibroblast apoptosis by anti-CD44 antibody: implications for the treatment of fibroproliferative lung disease. Am J Pathol 149: 1639–1650.
14. Bunek J, Kamarajan P, Kapila YL (2011) Anoikis mediators in oral squamous cell carcinoma. Oral Dis 17: 355–361.
15. Crockett RJ, Centrella M, McCarthy TL, Grant Thomson J (2010) Effects of cyclic strain on rat tail tenocytes. Mol Biol Rep 37: 2629–2634.
16. Takemura M, Itoh H, Sagawa N, Yura S, Korita D, et al. (2005) Cyclic mechanical stretch augments hyaluronan production in cultured human uterine cervical fibroblast cells. Mol Hum Reprod 11: 659–665.
17. Misra S, Obeid LM, Hannun YA, Minamisawa S, Berger FG, et al. (2008) Hyaluronan constitutively regulates activation of COX-2-mediated cell survival activity in intestinal epithelial and colon carcinoma cells. J Biol Chem 283: 14335–14344.
18. Gilmore AP (2005) Anoikis. Cell Death Differ 12: 1473–1477.
19. Darby IA, Bisucci T, Hewitson TD, MacLellan DG (1997) Apoptosis is increased in a model of diabetes-impaired wound healing in genetically diabetic mice. Int J Biochem Cell Biol 29: 191–200.
20. Martel H, Walker DC, Reed RK, Bert JL (2001) Dermal fibroblast morphology is affected by stretching and not by C48/80. Connect Tissue Res 42: 235–244.
21. Hsieh MH, Nguyen HT (2005) Molecular mechanism of apoptosis induced by mechanical forces. Int Rev Cytol 245: 45–90.
22. Swain Y (2005) The measurement of interface pressure. In: Bader DL, Bouten CVC, Colin D, Oomens CWJ, editors. Pressure ulcer research: Current and future perspectives. Heidelberg: Springer-Verlag. 51–88.
23. ZhaZn M, Zhao H, Han ZC (2004) Signalling mechanisms of anoikis. Histol Histopathol 19: 973–983.
24. Gilmore AP, Owens TW, Foster FM, Lindsay J (2009) How adhesion signals reach a mitochondrial conclusion ECM regulation of apoptosis. Curr Opin Cell Biol 21: 654–661.
25. Cheng TL, Symons M, Jou TS (2004) Regulation of anoikis by Cdc42 and Rac1. Exp Cell Res 95: 497–511.

26. Sreedhar AS, Csermely P (2004) Heat shock proteins in the regulation of apoptosis: new strategies in tumor therapy: a comprehensive review. Pharmacol Ther 101: 227–257.
27. Silver JT, Noble EG (2012) Regulation of survival gene hsp70. Cell Stress Chaperones 17: 1–9.
28. Fadeel B, Zhivotovsky B, Orrenius S (1999) All along the watchtower: on the regulation of apoptosis regulators. FASEB J 13: 1647–1657.
29. Bartling B, Tostlebe H, Darmer D, Holtz J, Silber RE, et al. (2000) Shear stress-dependent expression of apoptosis-regulating genes in endothelial cells. Biochem Biophys Res Commun 278: 740–746.
30. Riganò R, Profumo E, Buttari B, Tagliani A, Petrone L, et al. (2007) Heat shock proteins and autoimmunity in patients with carotid atherosclerosis. Ann N Y Acad Sci 1107: 1–10.
31. Tsutsumi S, Neckers L (2007) Extracellular heat shock protein 90: a role for a molecular chaperone in cell motility and cancer metastasis. Cancer Sci 98: 1536–1539.
32. Schnaider T, Oikarinen J, Ishiwatari-Hayasaka H, Yahara I, Csermely P (1999) Interactions of Hsp90 with histones and related peptides. Life Sci 65: 2417–26.
33. Itano N, Kimata K (1996) Molecular cloning of human hyaluronan synthase. Biochem Biophys Res Commun 222: 816–820.
34. Spicer AP, Augustine ML, McDonald JA (1996) Molecular cloning and characterization of a putative mouse hyaluronan synthase. J Biol Chem 271: 23400–23406.
35. Spicer AP, Olson JS, McDonald JA (1997) Molecular cloning and characterization of a cDNA encoding the third putative mammalian hyaluronan synthase. J Biol Chem 272: 8957–8961.
36. Smith WL, DeWitt DL, Garavito RM (2000) Cyclooxygenases: structural, cellular, and molecular biology. Annu Rev Biochem 69: 145–182.
37. Wang JH, Thampatty BP (2008) Mechanobiology of adult and stem cells. Int Rev Cell Mol Biol 271: 301–346.
38. Tong M, Tuk B, Hekking IM, Pleumeekers MM, Boldewijn MB, et al. (2013) Heparan sulfate glycosaminoglycan mimetic improves pressure ulcer healing in a rat model of cutaneous ischemia-reperfusion injury. Wound Repair Regen 21: 329–334.
39. Demiot C, Sarrazy V, Javellaud J, Gourloi L, Botelle L, et al. (2011) Erythropoietin restores C-fiber function and prevents pressure ulcer formation in diabetic mice. J Invest Dermatol 131: 2316–2322.
40. O'Loughlin A, Kulkarni M, Creane M, Vaughan EE, Mooney E, et al. (2013) Topical administration of allogeneic mesenchymal stromal cells seeded in a collagen scaffold augments wound healing and increases angiogenesis in the diabetic rabbit ulcer. Diabetes 62: 2588–2594.
41. Inoue H, Murakami T, Ajiki T, Hara M, Hoshino Y, et al. (2008) Bioimaging assessment and effect of skin wound healing using bone-marrow-derived mesenchymal stromal cells with the artificial dermis in diabetic rats. J Biomed Opt 13: 064036.
42. Renò F, Sabbatini M, Lombardi F, Stella M, Pezzuto C, et al. (2003) In vitro mechanical compression induces apoptosis and regulates cytokines release in hypertrophic scars. Wound Repair Regen 11: 331–336.
43. Yip CP, Walker D, Fernlund G, Pinder K (2007) Role of dermal fibroblasts in rat skin tissue biomechanics. Biomed Mater Eng 17: 109–117.
44. Maines MD (1997) The heme oxygenase system: a regulator of second messenger gases. Annu Rev Pharmacol Toxicol 37: 517–554.
45. Nakai A, Satoh M, Hirayoshi K, Nagata K (1992) Involvement of the stress protein HSP47 in procollagen processing in the endoplasmic reticulum. J Cell Biol 117: 903–914.
46. Gorman AM, Heavey B, Creagh E, Cotter TG, Samali A (1999) Antioxidant-mediated inhibition of the heat shock response leads to apoptosis. FEBS Lett 445: 98–102.
47. Gottlieb E, Vander Heiden MG, Thompson CB (2000) Bcl-x(L) prevents the initial decrease in mitochondrial membrane potential and subsequent reactive oxygen species production during tumor necrosis factor alpha-induced apoptosis. Mol Cell Biol 20: 5680–5689.
48. Roehlecke C, Kuhnt AK, Fehrenbach H, Werner C, Funk RH, et al. (2000) Resistance of L132 lung cell clusters to glyoxal-induced apoptosis. Histochem Cell Biol 114: 283–292.
49. Harper LJ, Costea DE, Gammon L, Fazil B, Biddle A, et al. (2010) Normal and malignant epithelial cells with stem-like properties have an extended G2 cell cycle phase that is associated with apoptotic resistance. BMC Cancer 10: 166.
50. Itano N, Sawai T, Yoshida M, Lenas P, Yamada Y, et al. (1999) Three isoforms of mammalian hyaluronan synthases have distinct enzymatic properties. J Biol Chem 274: 25085–25092.
51. Mascarenhas MM, Day RM, Ochoa CD, Choi WI, Yu L, et al. (2004) Low molecular weight hyaluronan from stretched lung enhances interleukin-8 expression. Am J Respir Cell Mol Biol 30: 51–60.
52. Kreger ST, Voytik-Harbin SL (2009) Hyaluronan concentration within a 3D collagen matrix modulates matrix viscoelasticity, but not fibroblast response. Matrix Biol 28: 336–346.
53. Gerdin B, Hällgren R (1997) Dynamic role of hyaluronan (HYA) in connective tissue activation and inflammation. J Intern Med 242: 49–55.
54. Coleman PJ, Scott D, Abiona A, Ashhurst DE, Mason RM, et al. (1998) Effect of depletion of interstitial hyaluronan on hydraulic conductance in rabbit knee synovium. J Physiol 509: 695–710.
55. Xin X, Borzacchiello A, Netti PA, Ambrosio L, Nicolais L (2004) Hyaluronic-acid-based semi-interpenetrating materials. J Biomater Sci Polym Ed 15: 1223–1236.
56. Falcone SJ, Palmeri DM, Berg RA (2006) Rheological and cohesive properties of hyaluronic acid. J Biomed Mater Res A 76: 721–728.
57. Evanko SP, Tammi MI, Tammi RH, Wight TN (2007) Hyaluronan-dependent pericellular matrix. Adv Drug Deliv Rev 59: 1351–1365.
58. Hardingham TE, Muir H (1972) The specific interaction of hyaluronic acid with cartilage proteoglycans. Biochim Biophys Acta 279: 401–405.
59. Hardingham TE, Fosang AJ (1992) Proteoglycans: many forms and many functions. FASEB J 6: 861–870.
60. Lee RT, Yamamoto C, Feng Y, Potter-Perigo S, Briggs WH, et al. (2001) Mechanical strain induces specific changes in the synthesis and organization of proteoglycans by vascular smooth muscle cells. J Biol Chem 276: 13847–13851.
61. Uchiyama H, Dobashi Y, Ohkouchi K, Nagasawa K (1990) Chemical change involved in the oxidative reductive depolymerization of hyaluronic acid. J Biol Chem 15: 7753–7759.
62. Minematsu T, Nakagami G, Yamamoto Y, Kanazawa T, Huang L, et al. (2013) Wound blotting: a convenient biochemical assessment tool for protein components in exudate of chronic wounds. Wound Repair Regen 21: 329–334.

Journal of Tissue Viability (2014) 23, 60–68

ELSEVIER

JOURNALOF
tissueviability

www.elsevier.com/locate/jtv

Basic research

Using an extreme bony prominence anatomical model to examine the influence of bed sheet materials and bed making methods on the distribution of pressure on the support surface

Terumi Iuchi [a], **Yukari Nakajima** [a], **Moriyoshi Fukuda** [a], **Junko Matsuo** [b], **Hiroyuki Okamoto** [c], **Hiromi Sanada** [d], **Junko Sugama** [e,*]

[a] *Department of Clinical Nursing, Division of Health Sciences, Graduate Course of Nursing Science, Kanazawa University, Kanazawa, Japan*
[b] *Faculty of Nursing, Osaka Medical College, Osaka, Japan*
[c] *Department of Quantum Medical Technology, Institute of Medical, Pharmaceutical and Health Sciences, Kanazawa University, Kanazawa, Japan*
[d] *Department of Gerontological Nursing/Wound Care Management, Division of Health Science and Nursing, Graduate School of Medicine, University of Tokyo, Japan*
[e] *Department of Clinical Nursing, Institute of Medical, Pharmaceutical and Health Sciences, Kanazawa University, 5-11-80 Kodatsuno, Kanazawa, Ishikawa 920-0942, Japan*

KEYWORDS
Pressure ulcer;
Pressure distribution;
Support surface;
Bed sheets;
Bed making

Abstract Bed sheets generate high surface tension across the support surface and increase pressure to the body through a process known as the hammock effect. Using an anatomical model and a loading device characterized by extreme bony prominences, the present study compared pressure distributions on support surfaces across different bed making methods and bed sheet materials to determine the factors that influence pressure distribution.

The model was placed on a pressure mapping system (CONFORMat®; NITTA Corp., Osaka, Japan), and interface pressure was measured. Bed sheet elasticity and friction between the support surface and the bed sheets were also measured.

* Corresponding author. Tel./fax: +81 76 265 2555.
E-mail address: junkosgm@mhs.mp.kanazawa-u.ac.jp (J. Sugama).

http://dx.doi.org/10.1016/j.jtv.2014.01.003

For maximum interface pressure, the relative values of the following methods were higher than those of the control method, which did not use any bed sheets: cotton sheets with hospital corners (1.28, $p = 0.02$), polyester with no corners (1.29, $p = 0.01$), cotton with no corners (1.31, $p = 0.003$), and fitted polyester sheets (1.35, $p = 0.002$). Stepwise multiple regression analysis indicated that maximum interface pressure was negatively correlated with bed sheet elasticity ($R^2 = 0.74$). A statistically significant negative correlation was observed between maximum interface pressure and immersion depth, which was measured using the loading device ($r = -0.40$ and $p = 0.04$).

We found that several combinations of bed making methods and bed sheet materials induced maximum interface pressures greater than those observed for the control method. Bed sheet materials influenced maximum interface pressure, and bed sheet elasticity was particularly important in reducing maximum interface pressure.

Introduction

A pressure ulcer is a localized injury to the skin and/or underlying tissue that usually appears over a bony prominence as a result of pressure or pressure in combination with shear stress [1]. Pressure ulcers frequently occur among elderly bedridden patients with extreme bony prominences; therefore, it is important to use a support surface, such as a two-layer pressure air mattress, to redistribute the tissue load over bony prominences [2,3].

Bed sheets serve to protect patients from infection and maintain comfort. However, they often cause a phenomenon known as the hammock effect [4] in which the bed covers and sheets may generate high surface tension across the support surface [4] that leads to increased pressure; for example, if a patient's buttocks are not immersed, the contact area between the buttocks and the support surface is reduced, and pressure is increased (Fig. 1). Although the principle of the hammock effect is well-known, the methods to reduce this phenomenon remain unknown in clinical practice. Therefore, we investigated the potentials of different bed sheet-related methods to redistribute pressure across a patient's body.

Matsuo et al. [5] previously suggested that bed making methods influence the hammock effect on the support surface. Other studies have reported that bed sheet materials promote the hammock effect. For example, Iizaka et al. [6] found that the elasticities of cushion covers influences the hammock effect in wheelchairs, and Nagano et al. [7]. reported on the influence of friction on this phenomenon. Although these studies showed that the hammock effect can be aggravated by bed making methods and bed sheet materials, no studies have been conducted to determine the differences among bed making methods and bed sheet materials in terms of pressure distribution on the support surface. Therefore, using an anatomical model characterized by extreme bony prominences, we compared pressure distributions on the support surface across different bed making methods and bed sheet materials and identified the factors that influence pressure distribution. We hypothesized that bed making methods and bed sheet materials influence the maximum interface pressure on the support surface.

Materials and methods

Model

We employed an anatomical model and a loading device described and validated by Matsuo et al. [8]. The Matsuo model was developed to evaluate support surfaces and quantify the hammock effect. This model was created by attaching polyurethane gel and a film to a resin model of an adult female pelvis (female pelvis 1/1 scale model®; Nihon 3B Scientific Corp., Niigata, Japan) with an intercristal diameter of 25.0 cm and an interspinal diameter of 24.0 cm. Polyurethane gel was used to mimic the soft tissue of the buttocks at thicknesses of 80 and 210 mm and stiffnesses of 0.08 and 0.46 megapascals (MPa) at the sacral and hip regions, respectively. A polyurethane film (thickness, 0.3 mm) was used to mimic skin on the model (Fig. 2).

The loading device was composed of an aluminum frame (length, 100 cm; width, 60 cm; and height, 73 cm). A vertical load was applied to the sacral region using a weight attached to a vertical column erected at the center of the frame. A load of 11 kg was applied and the pelvis was tilted by 30°; these parameters were calculated based on contact areas and interface pressures of the buttocks from pressure redistribution maps of elderly bedridden patients [8]. A spring

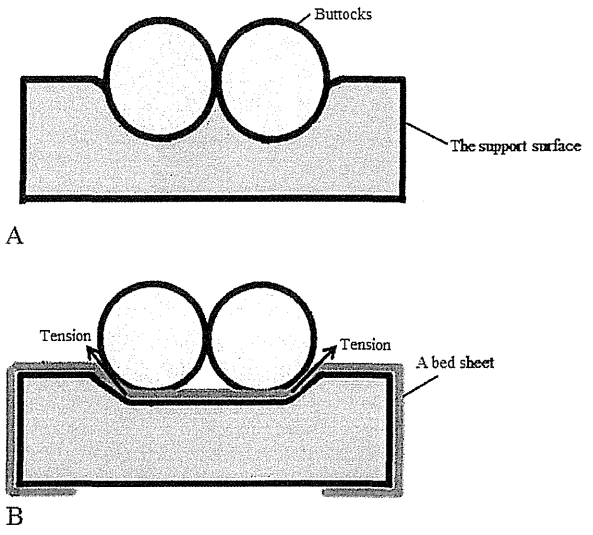

Figure 1 Theoretical model of the hammock effect on the support surface. (A) The situation without a bed sheet. (B) The situation with a bed sheet. Bed sheets generate high surface tension across the support surface such that the individual's buttocks are not immersed and the contact area between buttocks and support surface is reduced and pressure is increased.

was attached to the frame, and the anatomical model was fixed at an angle of 30° (Fig. 2) [8].

Support surface

A two-layer air mattress (Tricell®; Cape Ltd., Yokohama, Japan) with a reactive air mode consisting of a mattress (length, 191 cm; width, 84 cm; height, 10 cm), a pump, and a cover was used in the study. The mattress included 24 air cells, each of which was fabricated from 8-cm columnar polyurethane sheets. The cover was also made of polyurethane sheets. The internal pressure of the mattress was 25 mmHg, as described in a previous study [8], and the air in all cells was at the same internal pressure when the mattress activated. We selected an air mattress based on evidence that elderly bedridden patients may benefit from the use of a two-layer air mattress [3].

Bed making methods

We placed the support surface at the center of each bed sheet and drew a line at its center and outlined its shape on all bed sheets. Bed making was performed by one experimenter using three different methods: hospital corners, no corners, and fitted

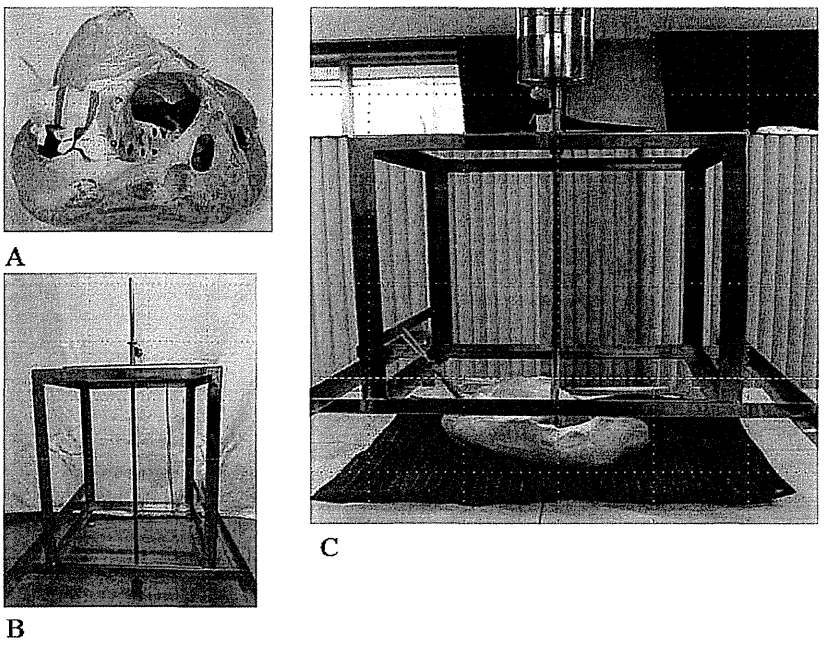

Figure 2 The anatomical model and loading device. (A) The anatomical model. It was made by attaching a polyurethane gel and film to a resin model of adult female pelvis. (B) The loading device. It consisted of an aluminum frame (length, 100 cm; width, 60 cm; and height, 73 cm). (C) The constructed model. By loading a weight onto a vertical column erected at the center of the frame, a vertical load could be applied to the sacral region. A load of 11 kg was then applied and the pelvis was tilted by 30°. A spring was attached to the frame, and the anatomical model was fixed at 30° angle.

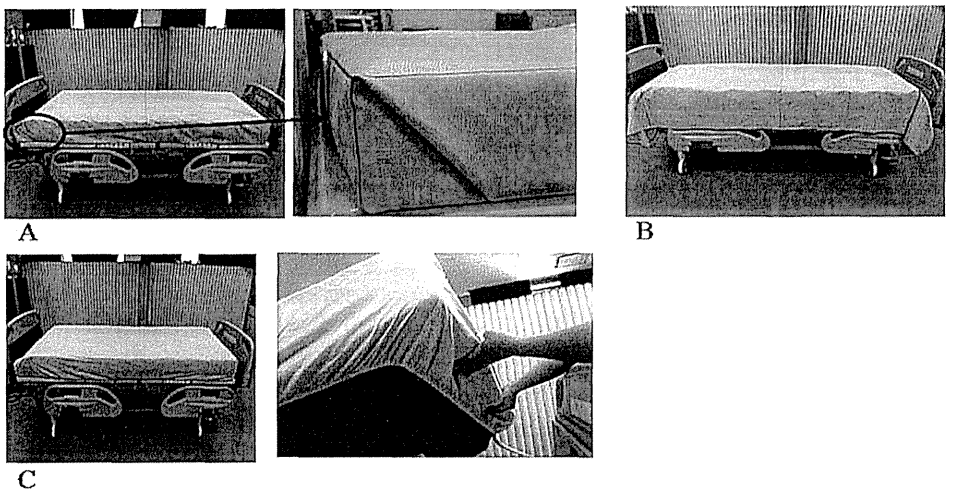

Figure 3 Bed making methods. (A) Hospital corners. The folded edge of the sheet formed a 45° angle from the corner on the surface of the bed. (B) No corners. We positioned a flat sheet over the support surface and did not tuck the edges. (C) Fitted sheets corners. We used fitted sheets.

sheet corners. In the first method, we positioned a flat sheet over the support surface, tucked the bottom edge under the mattress from corner to corner, and then folded one long edge onto the mattress so that the contour of the bed sheet was smooth at the corners and the folded sheet edge formed a 45° angle to the bed corner surface. In the second method, we spread a flat sheet over the support surface but did not tuck the edges in. In the third method, we used fitted sheets (Fig. 3).

Bed sheet types

Bed sheet types selected based on previous studies [5,6] and those used in clinical settings. We selected three types of bed sheets composed of materials with different elasticities: cotton, polyester, and polyester with a cotton pile (pile) (Table 1). Bed sheet elasticity was measured according to Japanese Industrial Standards (JIS L 1096). We measured the length- and width-wise elasticities of each bed sheet using calipers. Rectangular test pieces (30 × 6 cm) were cut from the bed sheets with the 30-cm edge parallel to either the length or the width of the bed sheets and attached to a loading frame as shown in Fig. 4. A 1-kg weight was suspended from each and, after 1 min, we measured the bed sheet length. Bed sheet elasticity was calculated as the change in the length of the longer side (i.e., the length of the longer side the weight had been attached for 1 min−30 cm (base line); Fig. 4).

Friction between the support surface and bed sheets

Both static and dynamic friction were measured. Static friction was measured using a bed sheet, a support surface cover, and two boards and two boards—a larger board (200 × 80 × 5 cm) to which we attached the cover and a smaller board (40 × 25 × 2.5 cm; weight, 1 kg) to which we attached the bed sheet. Next, we placed the smaller board over the larger board and slowly tilted them upward using a jack. When the smaller board began to slide down, we measured the angle of the larger board using a protractor. Static

Table 1 Types of bed sheets.

Types of bed sheets	Materials	Size (a length × a width × a height) (cm)
Cotton	Cotton 100%	Flat sheets: 150 × 260 × 0 Fitted sheets: 80 × 200 × 30
Polyester	Polyester 100%	Flat sheets: 150 × 250 × 0 Fitted sheets: 95 × 195 × 10
Pile	Pile: cotton 100%, Ground: polyester 100%	Flat sheets: 145 × 250 × 0 Fitted sheets: 100 × 200 × 25

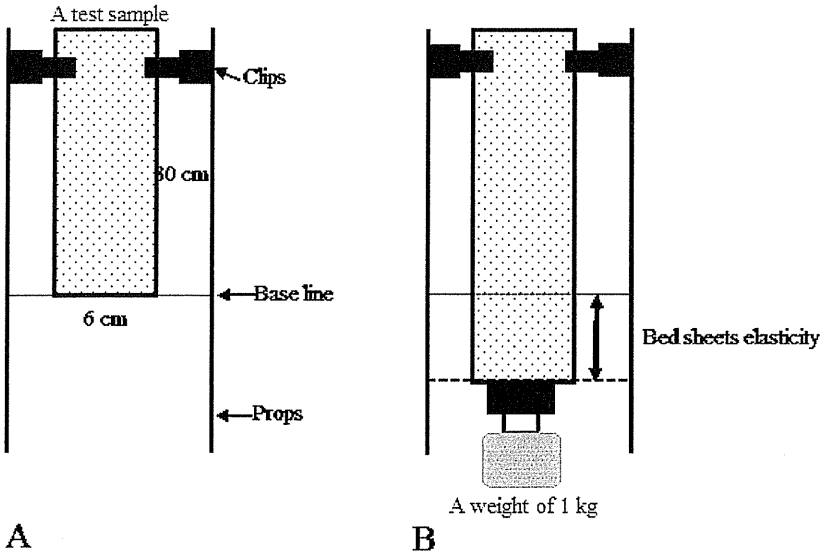

Figure 4 Bed sheet elasticity. (A) Before the measurement. Rectangular test pieces (30 × 6 cm) were cut from the bed sheets with the 30-cm edge parallel to either the length or the width of the bed sheets and attached to a loading frame. (B) A 1-kg weight was suspended from each. After 1 min, we measured the bed sheet length. Bed sheet elasticity was calculated as the change in the length of the longer side (i.e., the length of the longer side the weight had been attached for 1 min−30 cm (base line).

friction was calculated using the equation $F_1 = mg \sin\theta_{max} = \mu_1 mg \cos\theta_{max}$, where μ_1 is the coefficient of static friction, m is the weight of the smaller board (1 kg), g is 9.8 m/s^2 (constant), and θ_{max} is the angle of the larger board. From this formula, we calculated the static friction coefficient using the equation $\mu = \tan\theta_{max}$ for comparisons between the different types of bed sheets (Fig. 5) [9].

Dynamic friction was measured using a suspended weight (CUSTOM, Tokyo, Japan) to slowly pull the smaller board attached to the bed sheet against the larger board attached to the support surface cover. We attached the smaller board to the suspended weight and slid it over the larger board by pulling the suspended weight by hand. We measured the power expended when moving the smaller board using the suspended weight. Dynamic friction was calculated using the equation $F_2 = \mu_2 mg$, where μ_2 is the coefficient of dynamic friction, m is the weight of the smaller board (1 kg), and g is 9.8 m/s^2 (constant). Dynamic friction coefficients were calculated using the equation $\mu_2 = F_2/m \times 9.8$ (Fig. 5) [10].

Outcomes

The primary outcome of this study was maximum interface pressure, which was measured using a

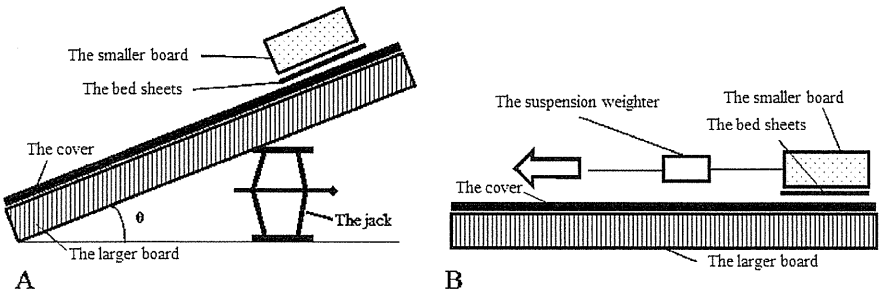

Figure 5 Friction between the support surface and bed sheets. (A) The methods of static friction. We put the smaller board on the larger board, and tilted the larger board slowly. When the smaller board began to slide down, we measured the angle (θ) of the larger board. (B) The methods of dynamic friction. We put the smaller board on the larger board and pulled the smaller board slowly. We measured the power expended when moving the smaller board using the suspended weight.

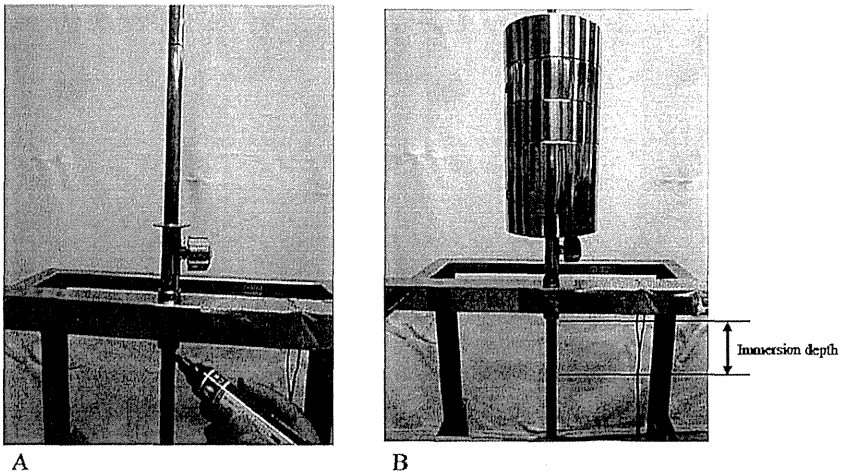

Figure 6 Measurement of the immersion depth into the support surface. (A) Before loading weights onto the anatomical model, a line was drawn on the column of the loading device. (B) After the experimentation. Another line was drawn, and the immersion depth was calculated as the difference in height between the two lines.

pressure mapping system (CONFORMat®; NITTA Corp., Osaka, Japan) that consists of a thin polyester pressure sensing mat (0.1 mm, 1024 flexible) and conformable sensors. The range of measurement of this system is 0–600 mmHg, and the accuracy is ±10%. Maximum interface pressure was defined as the average of the pressures of the cell with the highest pressure and the eight adjacent cells as described for anatomical model positions by Matsuo et al. [8].

The secondary outcome was immersion depth into the support surface, which was measured using the loading device described above. Before loading weight onto the anatomical model, a line was drawn on the column of the frame, and, after experimentation, a second line was drawn as described previously [8]. The distance between the two lines was measured using a ruler (Vernier Caliper®; Niigata Seiki Corp., Niigata, Japan; range of measurement, 0–150 mm; Fig. 6).

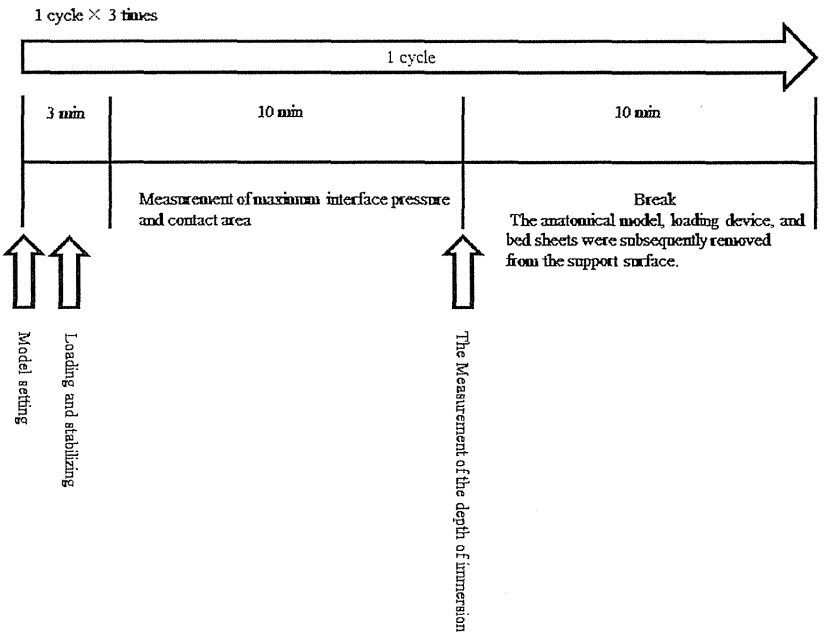

Figure 7 Measurement procedures.